

# Reconciling Observed and Predicted Tropical Rainforest OH Concentrations

### Key Points:

- OH observations with a chemical ionization mass spectrometer during the GoAmazon2014/5 study were lower than some previous studies
- Box model simulations of OH were carried out with five different chemical mechanisms
- Observed and model-predicted OH concentrations agree to within measurement uncertainty of 40%

### Supporting Information:

Supporting Information may be found in the online version of this article.











### Correspondence to:

S. Kim,  
saewungk@uci.edu

### Citation:

Jeong, D., Seco, R., Emmons, L., Schwantes, R., Liu, Y., McKinney, K. A., et al. (2022). Reconciling observed and predicted tropical rainforest OH concentrations. *Journal of Geophysical Research: Atmospheres*, 127, e2020JD032901. <https://doi.org/10.1029/2020JD032901>

Received 10 APR 2020  
Accepted 3 DEC 2021

Daun Jeong<sup>1,2</sup> , Roger Seco<sup>1,3</sup> , Louisa Emmons<sup>4</sup> , Rebecca Schwantes<sup>4,5,6</sup> , Yingjun Liu<sup>7,8</sup>,  
Karena A. McKinney<sup>7</sup> , Scot T. Martin<sup>7,9</sup> , Frank N. Keutsch<sup>7,10,11</sup> , Dasa Gu<sup>1,12</sup>,  
Alex B. Guenther<sup>1</sup> , Oscar Vega<sup>13</sup>, Julio Tota<sup>14</sup>, Rodrigo A. F. Souza<sup>15</sup>,  
Stephen R. Springston<sup>16</sup>, Thomas B. Watson<sup>16</sup> , and Saewung Kim<sup>1</sup> 

<sup>1</sup>Department of Earth System Science, School of Physical Sciences, University of California, Irvine, CA, USA, <sup>2</sup>Now at Department of Chemistry, University of Michigan, Ann Arbor, MI, USA, <sup>3</sup>Now at Department of Biology, University of Copenhagen, Copenhagen, Denmark, <sup>4</sup>Atmospheric Chemistry Observations and Modeling Laboratory, National Center for Atmospheric Research, Boulder, CO, USA, <sup>5</sup>Now at Cooperative Institute for Research in Environmental Sciences, University of Colorado, Boulder, CO, USA, <sup>6</sup>Now at Chemical Sciences Laboratory, National Oceanic and Atmospheric Administration, Boulder, CO, USA, <sup>7</sup>John A. Paulson School of Engineering and Applied Sciences, Harvard University, Cambridge, MA, USA, <sup>8</sup>Now at College of Environmental Sciences and Engineering, Peking University, Beijing, China, <sup>9</sup>Department of Earth and Planetary Sciences, Harvard University, Cambridge, MA, USA, <sup>10</sup>Department of Chemistry, University of Wisconsin-Madison, Madison, WI, USA, <sup>11</sup>Department of Chemistry and Chemical Biology, Harvard University, Cambridge, MA, USA, <sup>12</sup>Now at Hong Kong University of Science and Technology, Hong Kong, China, <sup>13</sup>Instituto de Pesquisas Energéticas e Nucleares, Cidade Universitária, São Paulo, Brazil, <sup>14</sup>Universidade Federal do Oeste do Pará, Santarém, Brazil, <sup>15</sup>Escola Superior de Tecnologia, Universidade do Estado do Amazonas, Manaus, Brazil, <sup>16</sup>Department of Environmental and Climate Sciences, Brookhaven National Laboratory, Upton, NY, USA

**Abstract** We present OH observations made in Amazonas, Brazil during the Green Ocean Amazon campaign (GoAmazon2014/5) from February to March of 2014. The average diurnal variation of OH peaked with a midday (10:00–15:00) average of  $1.0 \times 10^6 (\pm 0.6 \times 10^6)$  molecules  $\text{cm}^{-3}$ . This was substantially lower than previously reported in other tropical forest photochemical environments ( $2\text{--}5 \times 10^6$  molecules  $\text{cm}^{-3}$ ) while the simulated OH reactivity was lower. The observational data set was used to constrain a box model to examine how well current photochemical reaction mechanisms can simulate observed OH. We used one near-explicit mechanism (MCM v3.3.1) and four condensed mechanisms (i.e., RACM2, MOZART-T1, CB05, CB6r2) to simulate OH. A total of 14 days of analysis shows that all five chemical mechanisms were able to explain the measured OH within instrumental uncertainty of 40% during the campaign in the Amazonian rainforest environment. Future studies are required using more reliable  $\text{NO}_x$  and VOC measurements to further investigate discrepancies in our understanding of the radical chemistry in the tropical rainforest.

## 1. Introduction

Since Levy (1971) postulated the importance of hydroxyl radicals (OH) in driving the photochemistry of the troposphere, numerous modeling, laboratory, and field studies have explored its roles in determining the chemical lifetimes of reactive trace gases and producing photochemical products such as ozone ( $\text{O}_3$ ) and secondary aerosol precursors such as inorganic acids ( $\text{HNO}_3$  and  $\text{H}_2\text{SO}_4$ ) and oxygenated volatile organic compounds (OVOCs). Tropospheric OH is primarily produced through  $\text{O}_3$  photolysis and the following reaction of O (<sup>1</sup>D) and water vapor ( $\text{H}_2\text{O}$ ). The OH level is sustained by recycling processes through nitric oxide (NO) oxidation to nitrogen dioxide ( $\text{NO}_2$ ) by organic peroxy ( $\text{RO}_2$ ) and hydroperoxy ( $\text{HO}_2$ ) radicals, generated from the oxidation of VOCs (R1–R3). Cross ( $\text{HO}_2 + \text{RO}_2$ ) or self-reactions ( $\text{HO}_2 + \text{HO}_2$  or  $\text{RO}_2 + \text{RO}_2$ ) between peroxy radicals compete with R2 and R3 to produce more stable compounds such as organic hydroxy peroxides. At low  $\text{NO}_x$  and high VOC environments, regeneration of OH is suppressed by these chain terminating reactions. Therefore early studies of conventional chemistry speculated OH levels are depleted in remote tropical rain forests (Jacob & Wofsy, 1988; Logan et al., 1981).



However, numerous field observations in relatively clean forested regions have reported higher than model simulated OH concentrations, contrary to the conventional understanding of tropospheric photochemistry (Carslaw et al., 2001; Hofzumahaus et al., 2009; Lelieveld et al., 2008; Pugh et al., 2010; Ren et al., 2008; Stone et al., 2010; D. Tan et al., 2001; Thornton et al., 2002; Whalley et al., 2011). In an airborne study above the tropical forests in Suriname, Lelieveld et al. (2008) measured up to  $\sim 10$  times higher than expected OH in the boundary layer. During the Photochemistry, Emissions, and Transport (PROPHET) campaign in a deciduous forest in Michigan, observed OH was  $\sim 3$  times higher than model simulations while HO<sub>2</sub> showed reasonable agreement (D. Tan et al., 2001). At an isoprene dominated rural region in the Pearl River Delta, China, measured OH overestimated the conventional chemistry prediction by  $\sim 5$  times while HO<sub>2</sub> agreed within uncertainty (Hofzumahaus et al., 2009).

Novel OH recycling pathways were proposed to reconcile the observed OH levels (Archibald et al., 2010; Butler et al., 2008; Hofzumahaus et al., 2009; Kubistin et al., 2010; Taraborrelli et al., 2009). For example, Hofzumahaus et al. (2009) were able to reconcile the measured OH levels by forcing a hypothetical compound “X” that is equivalent to 0.85 ppb of NO in their model simulations. Laboratory experiments (Jenkin et al., 2007, 2010) indicated that reaction between RO<sub>2</sub> and HO<sub>2</sub>, which was previously thought to be a chain terminating reaction, could also produce OH. By assuming isoprene-derived peroxy radical chemistry, with an enhanced OH recycling efficiency, the model well predicted the observed OH level based on the airborne dataset from the boundary layer of a remote pristine rain forest over Surinam (Lelieveld et al., 2008). More recently, chemical reactions mechanisms, such as isoprene radical isomerization processes leading to series of reactions reproducing OH (Asatryan et al., 2010; Berndt et al., 2019; Crounse et al., 2011; Peeters et al., 2009, 2014; Peeters & Müller, 2010; Teng et al., 2017; Wolfe et al., 2012) have been proposed.

Alternative explanations for the higher than expected OH observations include positive artifacts associated with internally generated OH. Previous studies of OH measurements in high BVOC regions with the laser-induced fluorescence (LIF) technique have shown that this artifact can be as much as a factor of 3 (Feiner et al., 2016; Hens et al., 2014; Mao et al., 2012; Novelli et al., 2014). Using an alternative background determining approach, the chemical removal method, by adding propane (C<sub>3</sub>H<sub>8</sub>) or hexafluoropropylene (C<sub>3</sub>F<sub>6</sub>) in the inlet to scrub OH, Mao et al. (2012) reported up to four-fold lower observed OH concentrations than the conventional background characterization method. By applying this chemical removal method, the authors were able to account for the OH levels measured at the Blodgett Forest Research Station in the California Sierra Nevada Mountains, using box model calculations embedded with the Regional Atmospheric Chemistry Mechanism (RACM2) updated with additional isoprene hydroxyp peroxy radical isomerizations, suggested in previous studies (Crounse et al., 2011; Peeters et al., 2009). Novelli et al. (2014) also implemented this chemical removing method in their LIF-FAGE system in three different forested areas in Spain, Finland, and Germany. The authors found up to 30%–80% of OH overestimation from the recycling processes within the instrument. This study also reported that an OH intercomparison between the modified LIF and the Chemical Ionization Mass Spectrometer (CIMS), which also uses propane as a scavenger, showed good agreement between the different techniques. During the Southern Oxidant and Aerosol Study (SOAS), Feiner et al. (2016) conducted HO<sub>x</sub> measurements with the Ground-based Tropospheric Hydrogen Oxides Sensor (GTHOS) system using LIF, at a forested region near Brent, Alabama. Compared to the method without the chemical removal, their LIF system using C<sub>3</sub>F<sub>6</sub> measured  $\sim 3$  times less OH during the campaign. Comparison of measured OH between CIMS and LIF, with the chemical removal background technique, during the SOAS campaign showed agreement within instrument uncertainty of 40% (Sanchez et al., 2018). However, the extent of the instrumental interferences highly depends on the ambient conditions and details on the instrumental configurations. For instance, recent chamber and flow reactor experiments (Fuchs et al., 2016; Novelli et al., 2018; Rickly & Stevens, 2018) reported that ozonolysis of BVOCs and photooxidation of MBO by OH, which were suspected to cause internal interference within the LIF, likely generate negligible OH under atmospheric relevant conditions. Moreover, the interference has been shown to depend on the length of the inlet and the cell pressure of the instrument (Fuchs et al., 2016; Rickly & Stevens, 2018).

Nonetheless, extensive improvements in isoprene oxidation mechanisms have been made in the past decade (Bates & Jacob, 2019; Jenkin et al., 2015; Knote et al., 2014; Saunders et al., 2003; Wennberg et al., 2018). Near-explicit chemical mechanisms such as the Master Chemical Mechanism (MCM) (Jenkin et al., 2015; Saunders et al., 1997, 2003) and the recently reported mechanism by Wennberg et al. (2018) include the most recent laboratory results of detailed isoprene oxidation and the subsequent reaction of hydroxy peroxy radicals (i.e.,

ISOPOO) with other oxidants ( $\text{NO}$ ,  $\text{HO}_2$ ,  $\text{RO}_2$ ) and its isomerization reactions. Crouse et al. (2011) experimentally confirmed the generation of hydroperoxyenals (HPALDs) from isoprene oxidation by OH in a chamber experiment. Laboratory experiments by Wolfe et al. (2012) have confirmed that once produced,  $\text{C}_5$ -HPALDs can photolyze with a quantum yield of 1 (300–400 nm) to produce OH (yield = 1). Additional OH production from this isoprene radical isomerization reaction has been further supported by Fuchs et al. (2013) through an isoprene-oxidation chamber experiment with experimental conditions similar to the field sites in the Borneo rainforest and Pearl River Delta. The conventional chemistry in the MCM v 3.2 predicted OH a factor of 2 lower than the measurements while the model embedded with the unimolecular isoprene isomerization with rate constants based on the work, presented by Crouse et al. (2011), matched well. These reactions have now been included in MCM v3.3.1 (Jenkin et al., 2015) with adjusted rate coefficients (Crouse et al., 2014; Peeters 2015). Feiner et al. (2016) showed that box model simulations using the most recent MCM v3.3.1 were able to reproduce OH observations measured with the LIF, with the chemical background method, in an Alabama forest. However, even after considering the aforementioned observation interferences and additional isoprene oxidation schemes, there still remains uncertainties as shown in recent studies. In a chamber study by Novelli et al. (2020), model simulations with MCM v3.3.1 could not reproduce measured OH, especially in low  $\text{NO}_x$  conditions (<0.2 ppb). A field study in a rural area near Wangdu, China, Z. Tan et al. (2017) reported higher observed OH as much as a factor of two compared to OH simulated from the RACM 2 with additional isoprene chemistry (Crouse et al., 2012; Peeters et al., 2014), when NO was below 0.9 ppb.

For practical purposes, chemical mechanisms need to be more condensed to be used in global chemical transport models so that the host model framework can run efficiently (Goliff et al., 2013). Simplifications require lumping organic compounds with comparable structure or reactivity. It is important to find a reasonable compromise so that the simplified chemical mechanism system can properly simulate ambient photochemical processes and the choice of the type of condensed photochemical mechanisms in a model should be taken cautiously depending on specific research goals (Chen et al., 2010; Dodge, 2000; Gross & Stockwell, 2003; Jimenez et al., 2003; Knote et al., 2015; Kuhn et al., 1998). For instance, Knote et al. (2015) compared gas-phase reactions of seven chemical mechanisms used in chemical transport models. The model was constrained with the same emission and meteorology parameters, and the use of different chemical mechanisms resulted in differences in simulated OH and  $\text{HO}_2$  of up to 40% and 25%, respectively. The authors concluded that the discrepancies were mainly coming from differences in oxidation reactions of BVOC and nighttime chemistry.

The status quo motivates us to test out box model simulations of both near-explicit and condensed mechanisms and examine whether they reproduce reasonable levels of OH, especially in forested environments, where previous studies have shown significant discrepancies between the measured and modeled OH. Here, we present OH observation using a CIMS at the T3 site ~60 km to the west of Manaus, Brazil as part of the Green Ocean Amazon (GoAmazon2014/5) research initiative (Martin et al., 2017). This is the first OH dataset measured by a CIMS in a rain forest environment. A multiplatform field campaign was conducted in 2014 in two Intensive Operating Period (IOPs)—wet (I) and dry (II) seasons. The wet season (1 Feb–30 Mar) represents a pristine condition while the dry season (15 Aug–15 Oct) is relatively polluted from increased biomass burning. Further description of the different IOPs is described in Martin et al. (2016, 2017). We only present here the data from the first IOP. The T3 ground observation site served as a supersite to characterize trace gas and aerosol physical and chemical properties with frequent overpasses of the DOE G-1 research aircraft. The location of the T3 site was carefully selected to sample a wide spectrum of anthropogenic influences on the pristine background. Manaus, the largest city in the state of Amazonas, is ~60 km away and air pollution plumes were at times transported to the site during the field observation period. In order to quantitatively assess our current understanding of tropospheric photochemistry, measured OH levels are compared to observation-constrained box model simulations utilizing a suite of explicit and condensed gas-phase mechanisms.

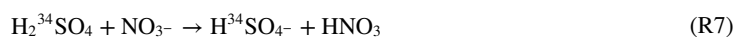
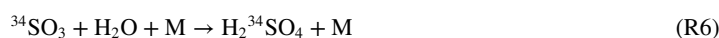
## 2. Materials and Methods

### 2.1. Chemical Ionization Mass Spectrometer

A THS Instruments LLC Atmospheric Pressure Chemical Ionization Mass Spectrometer (AP-CIMS) was used to quantify ambient OH with an instrument configuration identical to that deployed for the 2013 Southern Oxidant and Aerosol Study (SOAS) (Sanchez et al., 2018). The mass spectrometer was housed inside an air-conditioned shed at the T3 site. The inlet sampled outside ambient air at a height of 2 m above the ground. The analytical

method was developed by Tanner et al. (1997) and had mostly been used in low relative humidity environments such as the free troposphere (Mauldin et al., 1998), polar (Liao et al., 2011, 2012, 2014; Mauldin et al., 2010; Raso et al., 2017; Sjostedt et al., 2007), and nonurban regions (Kim, Kim, et al., 2015; Sanchez et al., 2018). During the past few years, the AP-CIMS has been deployed in high BVOC environments and compared with ambient OH concentration reported by using LIF instrumentation (Hens et al., 2014; Sanchez et al., 2018).

As thoroughly described in Tanner et al. (1997), the AP-CIMS technique for OH quantification draws bulk air flow into the inlet (1/2" OD metal tube) with a blower. From the center of the inlet flow, a sample flow of five standard liters per minute (slpm) is introduced to an injector system which consists of a pair of front and rear injectors. This allows injection of a mixture of gases to convert the sampled OH into sulfuric acid (H<sub>2</sub>SO<sub>4</sub>) (R4–R6). Background is characterized by adding excess pure C<sub>3</sub>H<sub>8</sub> for chemical removal of OH. In an ion reaction chamber, H<sub>2</sub>SO<sub>4</sub> is ionized by NO<sub>3</sub><sup>-</sup> reagent ion to produce HSO<sub>4</sub><sup>-</sup> (R7). NO<sub>3</sub><sup>-</sup> is generated by a corona discharge ion source unit described in Kürten et al. (2011) as a zero air stream doped with HNO<sub>3</sub> passes over the ion source. The generated analyte ion (HSO<sub>4</sub><sup>-</sup>) is introduced to a collision dissociation chamber (CDC), an octopole ion focus unit, and a quadrupole-channeltron ion detection unit, a typical configuration for mass spectrometry applications in atmospheric chemistry (Huey, 2007). A multipoint calibration was carried out as described in Sanchez et al. (2018). Briefly, OH was generated from photolysis (184.9 nm) of water in a ~30 slpm N<sub>2</sub> flow. The humidity in the calibration system was known and controlled by adjusting the fraction of N<sub>2</sub> flow being introduced to the water bubbler. The absolute water vapor concentration was measured by a Vaisala dew point and temperature probe (DMP 8) calibrated by a dew point generator (LI-610). The generated photons from a UV lamp (Pen-Ray 90-004-01) was calibrated by a Hamamatsu phototube (R5764) that was calibrated by the NIST calibration facility. The calibration was conducted on a weekly basis and the precision of the calibration factor was within 10% (1σ). The assessed limit of detection was 1 × 10<sup>5</sup> molecules cm<sup>-3</sup> and the uncertainty was 40% in 5 min for 2σ.



## 2.2. Box Model Simulations

The Framework for 0-D Atmospheric Modeling (FOAM v3.2) chemical box model was used to evaluate various chemical mechanisms for simulating OH levels during GoAmazon2014/5. FOAM is a MATLAB (Mathworks®) based zero-dimensional model framework (Wolfe, Marvin, et al., 2016), freely available at <https://github.com/AirChem/FOAM>. A more recent version of the model (v. 4.0) has been released, which includes bug fixes, additional model options, and chemical mechanisms, and the model results in this study are not expected to change with the modifications made in the newer version. It has been utilized to explore the oxidation chemistry in the troposphere with observational constraints from multiple community campaigns (Feiner et al., 2016; Jeong et al., 2019; Kaiser et al., 2016; Kim et al., 2015, 2016; Wolfe et al., 2014). The box model was constrained with a comprehensive set of trace gas and meteorology measurements collected during GoAmazon2014/5. The analytical techniques and references of the observational constraints used in this study are summarized in Table S1. Alkanes and alkenes that could not be quantified by PTR-ToF-MS were adapted from Zimmerman et al. (1988). Other parameters were measured during the campaign. A total of 14 days (12–14, 16–19 Feb, 5, 9, 11, 13, 15, 16, 18 March) were chosen during the campaign based on the availability of a complete dataset for the model simulations, excluding overcast and rainy days. Each diurnal cycle was constrained by inorganics (i.e., O<sub>3</sub>, NO<sub>2</sub>, CO), organics (i.e., CH<sub>4</sub>, biogenic and anthropogenic non-methane hydrocarbons), and meteorological parameters with a time step of 5 min. Alkanes and alkenes from Zimmerman et al. (1988) were constrained in the model with constant mixing ratios specified in Table S1.

NO<sub>x</sub> was not measured during the campaign due to technical difficulties along with NO<sub>x</sub> levels often being below detection limit (LOD: 50 ppt). Therefore, NO<sub>2</sub> was constrained in the model by assuming to be 6% of the observed NO<sub>y</sub>. Liu et al. (2016) extensively discussed the methodology to deduce NO from NO<sub>y</sub> using a box

**Table 1**  
*Chemical Mechanisms Used in Box Model Simulation of OH*

Mechanism	Number of species/reactions	3D model	Reference
MCM v3.3.1	<sup>a</sup> 5832/17,224		Jenkin et al. (2015)
MOZART-T1	159/328	<sup>b</sup> CAM-Chem, WRF-Chem	Knote et al. (2015) <sup>c</sup>
RACM2	124/363	for example., <sup>d</sup> CMAQ, <sup>e</sup> WRF-Chem	Goliff et al. (2013)
CB05	53/156	for example., CMAQ, WRF-Chem	Yarwood et al. (2005)
CB6r2	77/363	<sup>f</sup> CAMx	Ruiz and Yarwood (2013)

<sup>a</sup>Full mechanism. For the subset used in this study, 5,254 reactions and 1,694 species. <sup>b</sup>Community Atmosphere Model with Chemistry (CAM-chem), which is part of the NCAR Community Earth System Model (CESM). <sup>c</sup>A preliminary version of the MOZART-T1 as published in Knote et al. (2014). <sup>d</sup>Community Multiscale Air Quality system (CMAQ). <sup>e</sup>Weather Research and Forecasting Model with Chemistry (WRF-Chem). <sup>f</sup>Comprehensive Air quality Model with extensions (CAMx).

model and ground and airborne NO<sub>x</sub> dataset. They concluded that NO can be reasonably estimated for their purpose of interpreting ambient isoprene oxidation product distributions at the T3 site during the GoAmazon2014/5 campaign, where the OH observation was also conducted. Isoprene reacts with OH to produce ISOPOO, which can either react with HO<sub>2</sub> to produce hydroxyhydroperoxides (ISOPOOH) or with NO to produce methyl vinyl ketone (MVK) and methacrolein (MACR). The relative branching depends on the level of NO. The ratio ( $\xi$ ) of ISOPOOH to the sum of MVK and MACR, both measured during the campaign, was used to deduce the ratio of the corresponding production rates of each ( $\chi$ ). Based on the analysis by Liu et al. (2016),  $\xi$  was proportional to  $\chi$  and during background conditions (NO<sub>y</sub> < 1 ppb),  $\xi$  was 0.4–0.6 which corresponded to 0.6–0.9 of  $\chi$ . The dependence of  $\chi$  on NO was then simulated using box models embedded with MCM v3.3.1 and during background conditions, with  $\chi$  ranging 0.6–0.9, NO was deduced to be ~3% of NO<sub>y</sub>. The model simulated NO levels deduced by Liu et al. (2016) were well within previous NO measurements in the Amazon basin (Liu et al. (2016) and references therein). Airborne measurements during the campaign (DOI: <https://doi.org/10.5439/1346559>), when flying below 500 m, show a ratio of NO<sub>2</sub> to NO as 2.3 ± 1 (for 1 $\sigma$ ). Therefore, in our study, NO<sub>2</sub> was constrained in the box model as 6% of measured NO<sub>y</sub> and NO was determined in the model based on the photostationary state relationship.

For each day, we run the box model for two consecutive diurnal cycles, using the same constraints for each cycle. The first diurnal cycle is treated as a “spin-up.” Sensitivity tests show that the modeled OH from the 2nd and 10th diurnal cycles show similar results with both the slope and R<sup>2</sup> being 0.99 (Figure S1). Therefore, we report the second day of the diurnal cycle in this study. The hybrid method in the FOAM model was employed for photolysis rate constant calculations (J). This method calculates J values based upon assessed solar spectra from the Tropospheric Ultraviolet Visible radiation model (TUV v5.2) (Madronich & Flocke, 1998) along with cross sections and quantum yields from literature (Wolfe, Kaiser, et al., 2016). Since the calculation was conducted with a clear sky condition, the J values were scaled to total diffuse and direct radiation between 0.4 and 4  $\mu$ m, measured at the T3 site during the campaign. The clear sky solar radiation, that was used for this scaling, was derived by getting the profile of the clear sky solar radiation from the TUV model and scaling it to the maximum midday values observed during the campaign. No heterogeneous reactions were considered in the model. An additional first-order loss rate was applied to all species, with a lifetime of 6 h following Kaiser et al. (2016). This loss term accounts for physical processes not present in the model (advection, entrainment, and deposition) and is necessary to prevent build-up of long-lived oxidation products. The sensitivity tests illustrate that the choice of the lifetime between 6 and 24 h would not affect the OH concentration simulations (Figure S1).

Five separate mechanisms, which were readily available in the box model framework used in this study, were used for simulating OH: Master Chemical Mechanism (MCM v3.3.1), Model for Ozone and Related Chemical Tracers (MOZART-T1), Carbon Bond Mechanism (CB05), Regional Atmospheric Chemistry Mechanism (RACM2), and Carbon Bond 6 Mechanism (CB6r2). The total number of species and reactions of each mechanism and their implementation in 3-D model frameworks are summarized in Table 1. Specifics of lumping for each mechanism are presented in Table S2. All the presented box model runs were constrained with the identical set of chemical and meteorological parameters. The Box Model Extensions to Kinetic PreProcessor (BOXMOX) was used to run the MOZART-T1 mechanism since this mechanism was not included in FOAM. BOXMOX is an extension to the

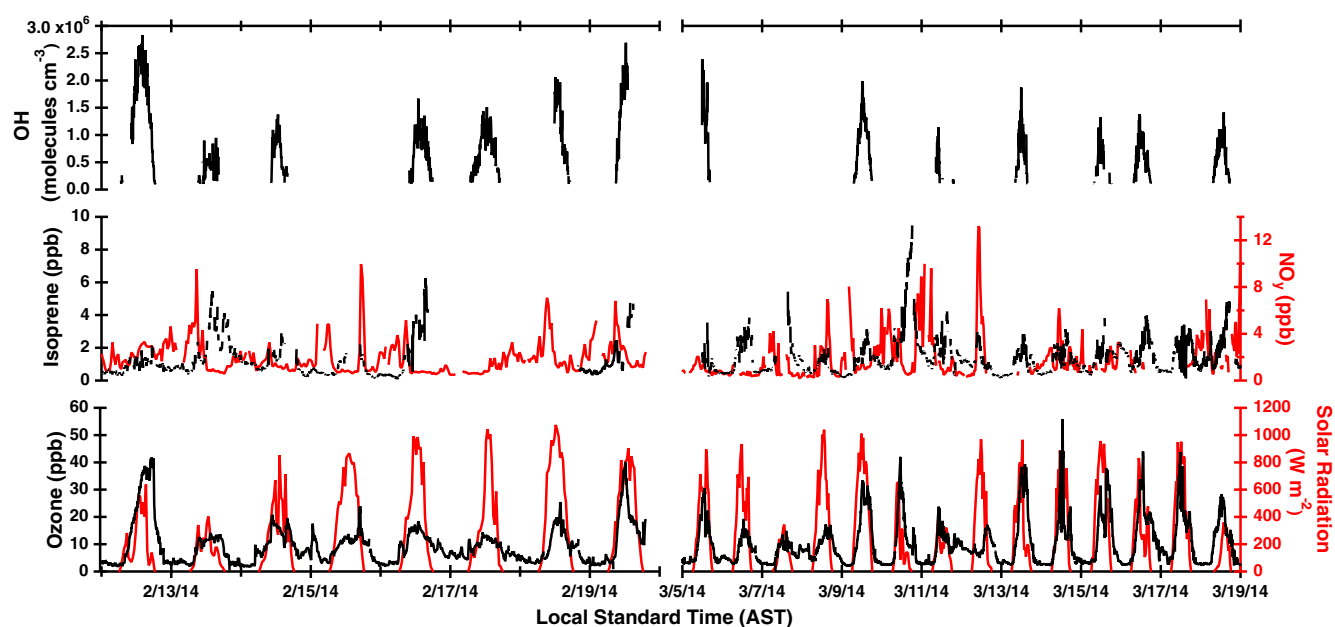


**Figure 1.** Temporal variation of OH, isoprene,  $\text{NO}_y$ ,  $\text{O}_3$ , and solar radiation during GoAmazon2014/5. The frequency of the data is 5 min for OH, isoprene, and  $\text{O}_3$  and 30 min for  $\text{NO}_y$  and solar radiation. Only the 14 days chosen for this study are presented for OH.

Kinetic PreProcessor (Knote et al., 2015) that uses a Rosenbrock solver. Comparisons between the two box models embedded with the identical MCM v3.3.1 mechanisms and observational constraints showed good agreement (Figure S2), which justify the comparisons of the model results between the two different model frameworks.

### 3. Results

#### 3.1. Observation Results During GoAmazon2014/5

Figure 1 shows the 14 days of OH data set used in this study. Bakwin et al. (1990) reported background conditions of  $\text{NO}_y$  in the Amazon rainforest during the wet season to be below 1 ppb based on the probability distribution of data collected from the whole observation period (April to May of 1987). As shown in the variation of  $\text{NO}_y$  in Figure 1, enhanced levels of  $\text{NO}_y$  were frequently observed, most likely from pollution plumes from Manaus. Diurnal averages and SDs of the 14 days of measured isoprene, total MVK and MACR, monoterpene, toluene, benzene, and CO are shown in Figure 2. Based on the observations of VOCs, isoprene is the most dominant OH sink in this environment consisting about 56% of midday OH reactivity (Figure S5).

The observed midday averaged OH level is significantly lower than those from the previous field campaigns in similar photochemical environments as shown in Table 2. Among the examples, GABRIEL, PROPHET, OP3, and Wangdu reported substantially higher OH than the CABINEX, BEARPEX09, SOAS, and GoAmazon2014/5. BEARPEX09 and SOAS used chemical removal method in their LIF system to determine background OH. During CABINEX and the study in Wangdu, chemical removal method was tested out and the interferences were concluded to be within the instrumental uncertainty. The campaigns presented in Table 2, regardless of geographical differences, have two similarities. First, biogenics are the dominant OH sink among the quantified trace gases. Second, NO is below 100 ppt and close to 50 ppt and so can be categorized as a low-to-moderate NO regime based on the expected fate of peroxy radicals. In the case of the Wangdu study, it was at a rural site near (<200 km) some large cities and therefore had a higher  $\text{NO}_x$  level. For the BEARPEX 09 site, the local emissions were mostly 2-methyl-3-buten-2-ol (MBO) and monoterpenes but isoprene was transported to the site from a nearby oak woodland area in the afternoon (Mao et al., 2012). OH reactivity, which is the inverse of OH lifetime, was relatively lower in PROPHET, CABINEX, Wangdu, and GoAmazon than other campaigns in Table 2.

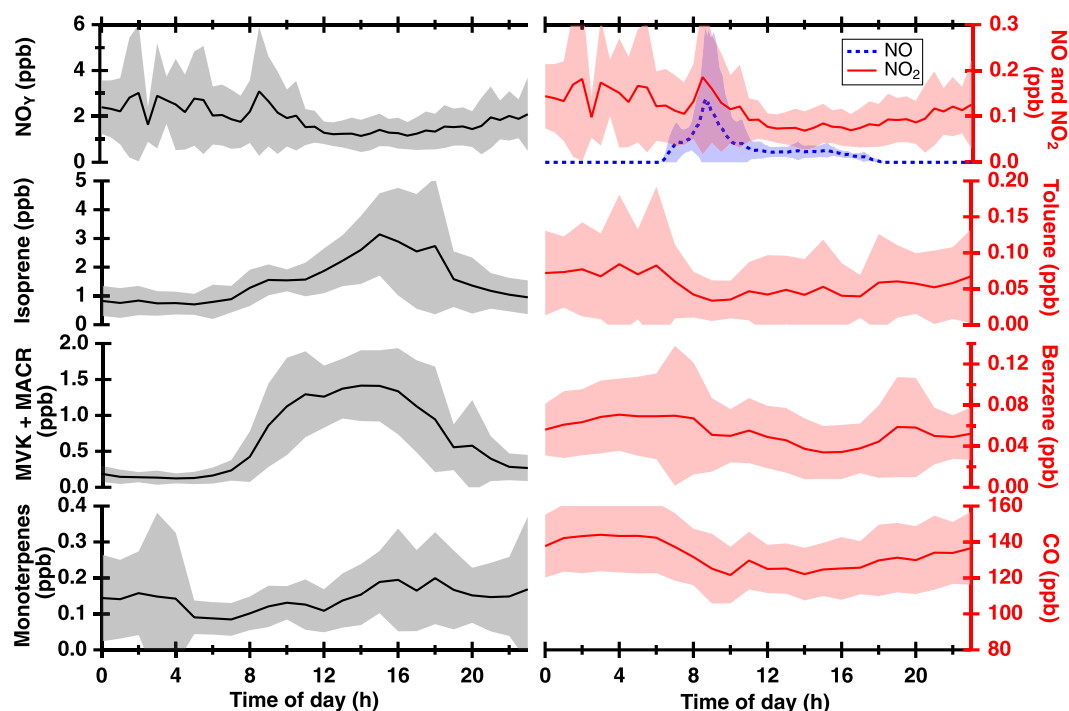


**Figure 2.** Diurnal variation of measured and estimated trace gases averaged over the 14 days used in this study. Shaded areas are SDs of the averages. NO<sub>2</sub> was estimated from measured NO<sub>y</sub> and NO was simulated from box model simulations with MCM v3.3.1.

**Table 2**

Summary of OH and Other Trace Gas Measurements From Various Field Campaigns Conducted in High Isoprene and Low-Moderate NO Environments

	<sup>a</sup> GABRIEL (October 2005)	<sup>b</sup> PROPHET (August 1998)	<sup>c</sup> OP3 (April- May 2008)	<sup>d</sup> CABINEX (July–August 2009)	<sup>e</sup> Wangdu (June–July 2014)	<sup>f</sup> BEARPEX09 (June–July 2009)	<sup>g</sup> SOAS (June–July 2013)	GoAmazon (February–March 2014)
Analytical Technique	LIF	LIF	LIF	<sup>h</sup> LIF	<sup>h</sup> LIF	<sup>h</sup> LIF	<sup>h</sup> LIF	CIMS
Averaged Time (LST)	14:00–17:00	10:00–11:00	11:00–12:00	11:00–14:00	12:00–16:00	09:00–15:00	10:00–15:00	10:00–15:00
CO (ppb)	122	260	111	260	540	130	134	121
OH (molec cm <sup>-3</sup> )	4.4 × 10 <sup>6</sup>	3.6 × 10 <sup>6</sup>	2.2 × 10 <sup>6</sup>	1.3 × 10 <sup>6</sup>	6.9 × 10 <sup>6</sup>	1.3 × 10 <sup>6</sup>	1.2 × 10 <sup>6</sup>	1.0 × 10 <sup>6</sup> ± 0.6 × 10 <sup>6</sup>
Isoprene (ppb)	4.3	1.86	2	1	0.84	1.7	5.14	2.25
MVK + MACR (ppb)	1.6	0.34	0.21	0.5	0.71	0.79	1.41	1.34
NO (ppt)	13	80	40	50	250	74	42	<sup>i</sup> 27 ± 25
NO <sub>2</sub> (ppt)		456	130	220	3,300	200	293	<sup>i</sup> 85 ± 50
O <sub>3</sub> (ppb)	17	41	12.5	30	93	54	37	21
OH reactivity (s <sup>-1</sup> )	19	11	19.8	12	11	18.5	21.1	8.5 ± 1.4

*Note.* The averaged dataset (or median if applicable) from GABRIEL, PROPHET, OP3, and BEARPEX09 are taken from Rohrer et al. (2014). Values from the CABINEX campaign and the study at Wangdu were estimated from Griffith et al. (2013) and Z. Tan et al. (2017), respectively.

<sup>a</sup>Tropical forest in Suriname, Guyana and Guyane (Lelieveld et al., 2008). <sup>b</sup>Deciduous forest in northern Michigan (D. Tan et al., 2001). <sup>c</sup>Danum Valley in the Sabah region of a Borneo forest (Whalley et al., 2011). <sup>d</sup>Deciduous forest in northern Michigan (Griffith et al., 2013). <sup>e</sup>Botanical garden in a rural site in Wangdu, North China Plain (Z. Tan et al., 2017). <sup>f</sup>Ponderosa pine plantation in the California Sierra Nevada Mountains (Mao et al., 2012). <sup>g</sup>Talladega National Forest in Brent, Alabama (Feiner et al., 2016). <sup>h</sup>Chemical removal method for determining background OH conducted during the observation period or tested out after the campaign. <sup>i</sup>NO<sub>2</sub> was estimated as 6% of observed NO<sub>y</sub> and NO is averaged from box model simulations with the MCM v3.3.1.

### 3.2. Comparison Between Observed and Modeled OH

With the observational dataset collected during GoAmazon2014/5, box model simulations were run for five different chemical mechanisms. Figure 3 shows the model simulation results along with the OH observations on the corresponding day. In most of the days, all five chemical mechanisms (i.e., MCM v3.3.1, RACM2, CB05, CB6r2, and MOZART-T1) generally agreed well with the OH measurements within the instrumental uncertainty. Among the 14 days presented in this study, 12 days (12, 13, 14, 16, 17, 18, 19 February, 5, 9, 11, 13, 16 March) showed model estimates were within uncertainty of the OH observations for most of the day except 18th March and 15th March. For 18th March, the five model simulations underestimated the observations up to fivefold. For 15th March, all mechanisms overestimated the measurements up to threefold. The agreement between the model simulations and the observations were the highest at midday with more discrepancies earlier or later in the day, which is consistent with the findings reported by Sanchez et al. (2018) for the SOAS dataset. Figure 4 shows correlation between OH observations and model results from five different chemical mechanisms. The red lines are linear trend lines of the correlations between modeled and observed OH. The results illustrate that the agreement is in general within the 40% uncertainty of the measurement throughout the OH range for the model runs with MCM v3.3.1, CB05, CB6r2, RACM2, and MOZART-T1 mechanisms. This finding is consistent with Mao et al. (2012) and Feiner et al. (2016) where they reconciled the observed OH with model simulations. During BEARPEX09, Mao et al. (2012) measured OH with the LIF using the chemical removal method at a ponderosa pine forest in Sierra Nevada. In their study, the authors were able to reconcile the observed levels of OH through box model simulations embedded with the RACM 2 mechanism with additional isoprene chemistry. An identical conclusion was presented by Feiner et al. (2016) with the SOAS dataset where they compared observations with box model runs with MCM v3.3.1. Indeed, the OH reactivity during GoAmazon2014/5 was relatively low, which could lead to a less pronounced production of unexplained OH if there were any. Rohrer et al. (2014) summarized previous field campaigns with high OH reactivity ( $>10 \text{ s}^{-1}$ ) and showed that unexplained OH production persisted in low  $\text{NO}_x$  environments compared to studies in pristine environments with low OH reactivity (e.g., Holland et al., 2003). In addition, according to Mao et al. (2012) and Novelli et al. (2017), the interference from the wave modulation method in LIF was more pronounced with increasing OH reactivity and temperature, which is indicative of higher terpene emissions. SOAS and BEARPEX were carried out in a high OH reactivity environment (Table 2) and observed up to a factor of 3 of interference from the wave modulation method compared to the chemical removal method. In comparison, CABINEX and Wangdu had lower OH reactivities, more similar to GoAmazon2014/5, and reported interferences within instrumental uncertainty and the model simulations still matched the observations generally well. On the other hand, it is also possible that the total OH reactivity during GoAmazon2014/5 was higher than the model simulations in this study. The model simulations only account for the constrained compounds and its oxidation products within the chemical schemes of each reaction mechanism. Any unidentified or unobserved compounds are therefore not considered in the modeled OH reactivity. However, our midday averaged total OH reactivity ( $\sim 8 \text{ s}^{-1}$ ), simulated by an observationally constrained box model, corresponds to what Nolscher et al. (2016) measured near the ground ( $\sim 7 \text{ s}^{-1}$ ) of the Amazon rainforest and inside the canopy ( $\sim 10 \text{ s}^{-1}$ ) during the wet season. In our study, isoprene was the dominant sink for OH, accounting for  $\sim 56\%$  of simulated total OH reactivity in the midday (Figure S5). This is consistent to Nolscher et al. (2016) where they reported that 60% of the total measured OH reactivity was explained by isoprene during the wet season at midday. Moreover, their study reported that missing OH reactivity at midday during the wet season was on average 5%–15%, within the uncertainty (16%) of the measurement. Therefore, we don't think the discrepancy between the modeled and measured OH reactivity would be significant in our study since the observations were carried out during the wet season. During GoAmazon2014/5 we did not see a clear trend in the extent of discrepancy between modeled and observed OH with respect to the level of isoprene (Figure S10). A follow up study in a similar environment with higher isoprene levels is required to directly measure total OH reactivity and compare them to previous studies with higher OH reactivity.

One uncertainty in the model runs originates from how  $\text{NO}_x$  is treated in the simulations. As described in Section 2,  $\text{NO}_2$  was assumed to be a fixed 6% of observed  $\text{NO}_y$ . However, these assumptions are based on background conditions and the ratio of  $\text{NO}$  to  $\text{NO}_y$  could vary, which could result in substantial changes in simulated OH level if the model is sensitive to constrained  $\text{NO}_2$ . Among the OH measurement used in this study, 35% of data points were during the background conditions of  $\text{NO}_y$  ( $<1 \text{ ppb}$ ). The diurnal variations of measured  $\text{NO}_y$  and estimated  $\text{NO}_x$  for each case day are summarized in Figure S4. Moreover, since  $\text{NO}$  was assumed to be in photostationary state with  $\text{NO}_2$ , if there were any significant source of fresh  $\text{NO}$  emissions near the observation site, for example,



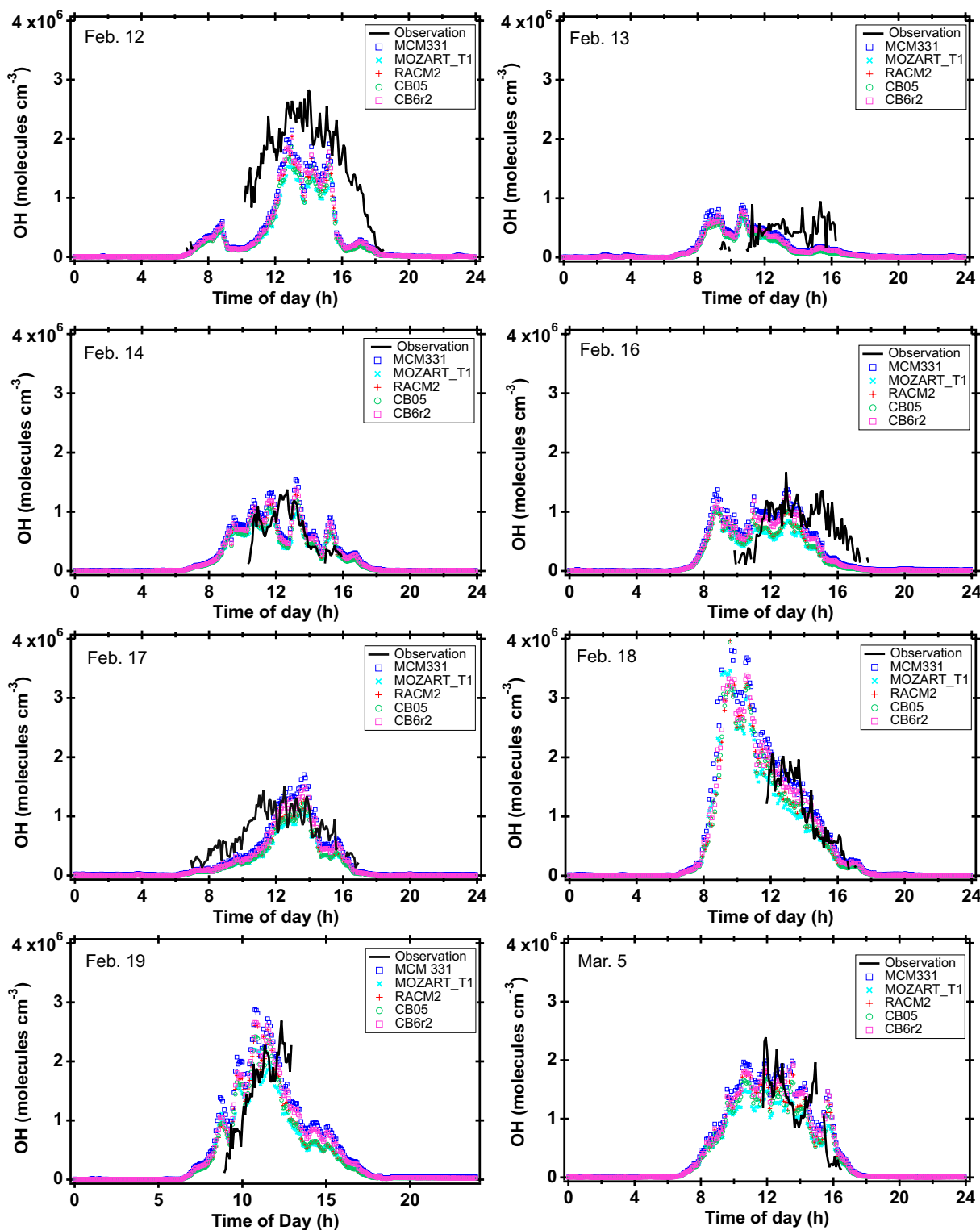


**Figure 3.** Comparison of measured and modeled OH during the GoAmazon2014/5 campaign. The box model simulations of OH were embedded with five different chemical mechanisms. The black line is the 5 min averaged OH observation results and gray shades are 40% instrumental uncertainty of the CIMS measurement. The frequency of the model simulations (markers) is 5 min.

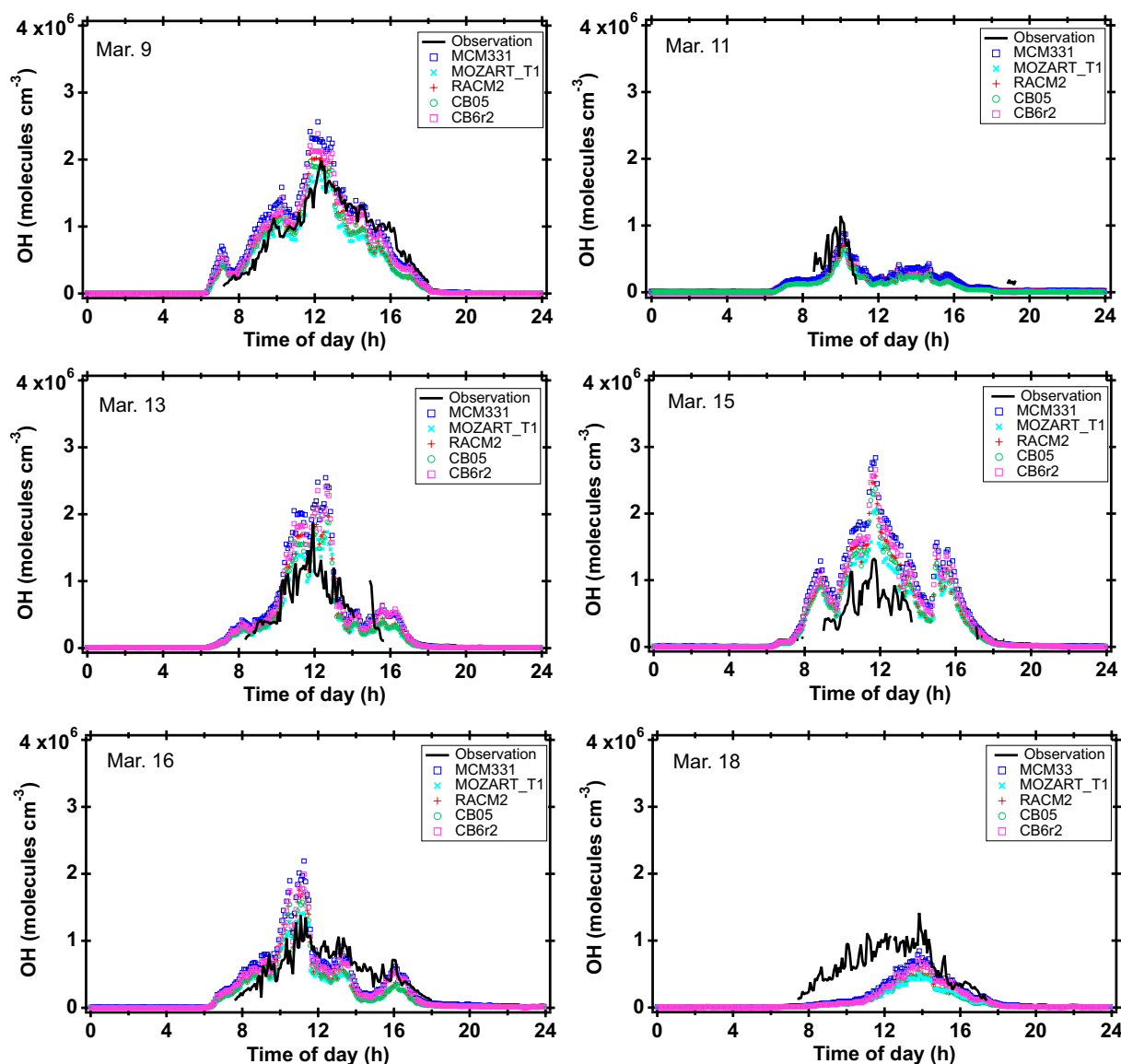
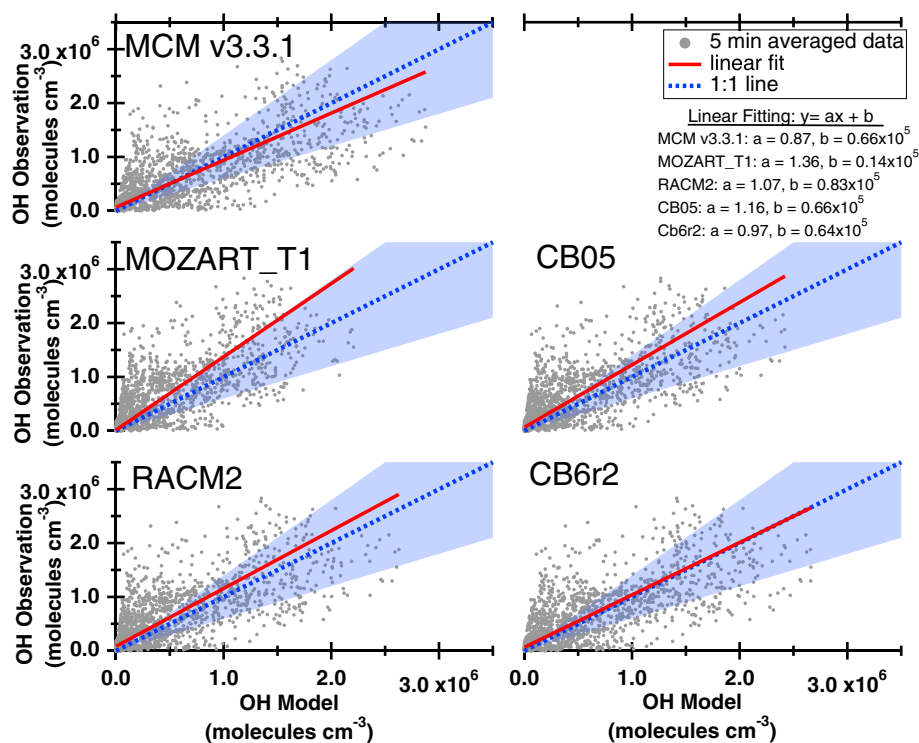


Figure 3. Continued.

from soils (Alaghmand et al., 2011), this could lead to uncertainties in modeled OH. NO emission from Manaus, however, is expected to reach photostationary state by the time it reaches the observation site, which is several hours downwind (Liu et al., 2016). In order to examine the potential uncertainties in the model caused by the  $\text{NO}_x$  estimation method applied in this study, sensitivity tests were carried out by constraining different  $\text{NO}_2$  levels in the model embedded with MCM v 3.3.1. As in Figure 5(a), doubling the constrained  $\text{NO}_2$  resulted in  $\sim 40\%$  higher OH at midday. Although this is within the instrumental uncertainty, it illustrates that the simulated OH is sensitive to how  $\text{NO}_2$  is constrained in the model runs. Quadrupling the constrained  $\text{NO}_2$  resulted in a factor of  $\sim 2.5$  of midday OH. For example, on 14th March, which was not included in the 14 selected days, midday  $\text{NO}_y$  ranged between 1 and 3 ppb. OH model simulations constrained with observation from 14th March, resulted in an overestimation of approximately three- to fivefold compared to observations. This is above the background  $\text{NO}_y$  levels and the airmasses were likely affected by pollution from Manaus, as shown in the back trajectories in Liu et al. (2016). Therefore, deriving NO as 3% of measured  $\text{NO}_y$  might not be applicable in some observation periods selected for the model simulations in Figure 3. However, we were not able to identify a clear dependence of the discrepancy between measured and modeled OH with varying  $\text{NO}_x$  levels as presented in later parts of the discussion (Figure 7b). We acknowledge that the lack of NO and  $\text{NO}_2$  observations during GoAmazon2014/5 is



**Figure 4.** Scatterplot of observed and simulated OH of five different chemical mechanisms. The blue dashed line is a 1:1 line with a 40% instrumental uncertainty in shades. Each gray marker is a 5 min data point and the red lines are the orthogonal distance regression fit between observed and modeled OH. 5 minute averaged observation results below detection limit were included in the analysis.

a critical limitation in carrying out a more detailed analysis and future studies with reliable NO<sub>x</sub> observations are imperative. It should also be noted that the small alkane and alkene concentrations taken from Zimmerman et al. (1988) could be a source of uncertainty. However, sensitivity runs in Figure 5(b), by doubling or halving the alkanes and alkene input concentrations rarely make a difference in the simulated OH, as isoprene is the most significant chemical sink of OH (Figure S5). Another feature shown in about half of the simulated days (i.e., 12, 13, 16, 19 February, and 9, 15 March) is the early morning peak of OH in the model results that occurred around 8:00–9:00 local standard time (Figure 6). These corresponded to a sudden peak in observed NO<sub>y</sub> levels, which could be from entrainment of the residual layer or influence of plume originating from Manaus. The NO<sub>x</sub> estimation method used in our model runs, which assumes a background condition of NO<sub>y</sub>, could be invalid at these times.

Figure 7 illustrates the relationship between modeled and observed OH for the selected 14 days as a function of other parameters such as JO<sup>1</sup>D, NO<sub>2</sub>, isoprene, and O<sub>3</sub>. Each line with markers is the binned median values of OH from observations (dashed line) and model runs (solid line) of five different chemical mechanisms with respect to each parameter. In order to avoid bias near the detection limit, OH observations below the instrumental detection limit were included in the analysis when deriving binned median values in Figure 7. The 5 min averaged observation data is also presented for comparison. The results show that the binned median of modeled OH from all five chemical mechanisms show reasonable agreement within the observation uncertainties throughout the whole range of photolysis (Figure 7a), which is consistent to what Feiner et al. (2016) reported during the SOAS campaign. According to Liu et al. (2018), noontime OH concentrations during GoAmazon2014/5 showed a positive correlation to noontime NO<sub>y</sub> for IOP I (wet season) and II (dry season) periods. In our study, modeled and observed OH levels, measured throughout the 14 days, increased up until 0.2 ppb of model input NO<sub>2</sub>, which is equivalent to ~3 ppb of measured NO<sub>y</sub> (Figure S6). Since solar radiation has a strong effect on OH (Figure 7a), correlation between input NO<sub>2</sub> and OH was color coded with JO<sup>1</sup>D (Figure 7b). Midday JO<sup>1</sup>D, calculated with the FOAM model, ranged between 1 and 5 × 10<sup>-5</sup> s<sup>-1</sup> (Figure S9). In background conditions (NO<sub>y</sub> < 1 ppb), about 35% of the observed OH (189 points among 539 points of 5 min averaged data) was when JO<sup>1</sup>D was above

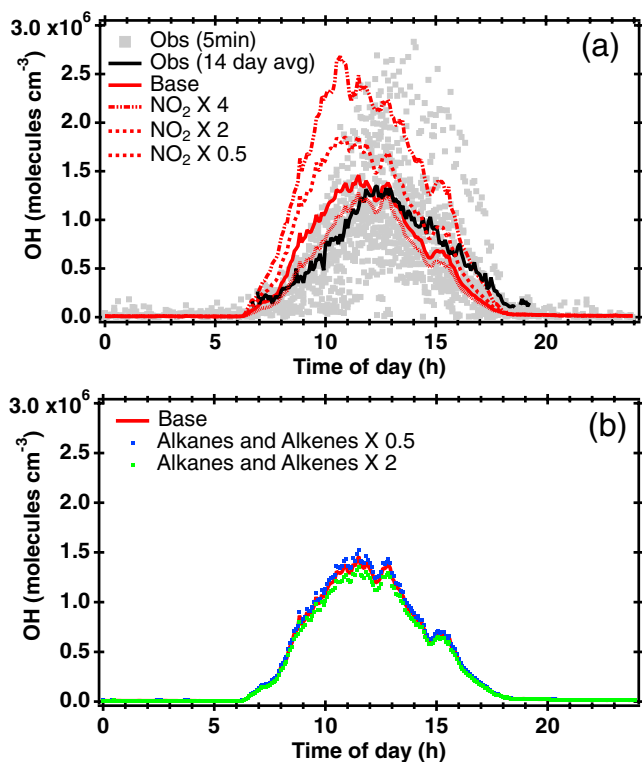


**Figure 5.** Sensitivity of modeled OH to varying levels of (a)  $\text{NO}_2$  and (b) VOC (i.e., alkanes and alkenes), simulated with FOAM v3.2 box model embedded with MCM v3.3.1 mechanism. 5 minute averaged OH observation data (gray marker in (a)) below detection limit is included. Only the data above detection limit is used for the averaged diurnal variation of measured and modeled OH.

$2 \times 10^{-5} \text{ s}^{-1}$ . Therefore, the lower levels of OH in background conditions were not just driven by weaker solar radiation. For other parameters, the median of the model results showed agreement within uncertainty below 5 ppb of isoprene (Figures 7d) and 35 ppb of  $\text{O}_3$  (Figure 7c), where they started to diverge. Because median values from when the divergence occurred are based on fewer data points than other bins, which showed good agreement, the bias may not be statistically relevant. However, one should note that as shown in the sensitivity tests illustrated in Figure 5, the model is sensitive to levels of  $\text{NO}_x$  and the  $\text{NO}_x$  levels estimated from relatively polluted air masses with high levels of  $\text{NO}_y$  are more uncertain compared to that from background air masses with low levels of  $\text{NO}_y$ . According to the chamber study by Novelli et al. (2020), modeled OH with MCM v3.3.1 still underestimated the measured OH in NO conditions below 0.2 ppb. During GoAmazon2014/5 both MCM v3.3.1 and condensed mechanisms were able to simulate OH within the instrumental uncertainties of measured OH in background conditions (i.e.,  $\text{NO}_2 < 60 \text{ ppt}$ ) as shown in Figure 7b. As model constrained  $\text{NO}_2$  was derived from measured  $\text{NO}_y$ , assuming background conditions, the 35% of the OH data points which were collected during background would have less uncertainty in the model simulations than above background conditions.

### 3.3. Comparison of Chemical Mechanisms

Figure 8a shows comparison of steady state model simulation of midday (11:00–13:00) OH from MCM v3.3.1 and other mechanism (CB05, CB6r2, RACM2). Based on the linear correlation, modeled OH from the three condensed mechanisms were 6%–15% lower than MCM v3.3.1. Since the OH reactivity, which is inverse of the lifetime of OH, is similar between mechanisms (Figure 8b), the discrepancies in the steady state modeled OH should result from differences in OH production rate. Model simulations of midday  $\text{HO}_2$  levels are compared between MCM v3.3.1 and other mechanisms in Figure 8c. RACM2 resulted in about 25% less  $\text{HO}_2$  than other mechanisms. This is consistent with what Wolfe, Kaiser, et al. (2016) presented and is due to lower  $\text{HO}_2$  production rates. RACM2 has a factor of two lower reaction

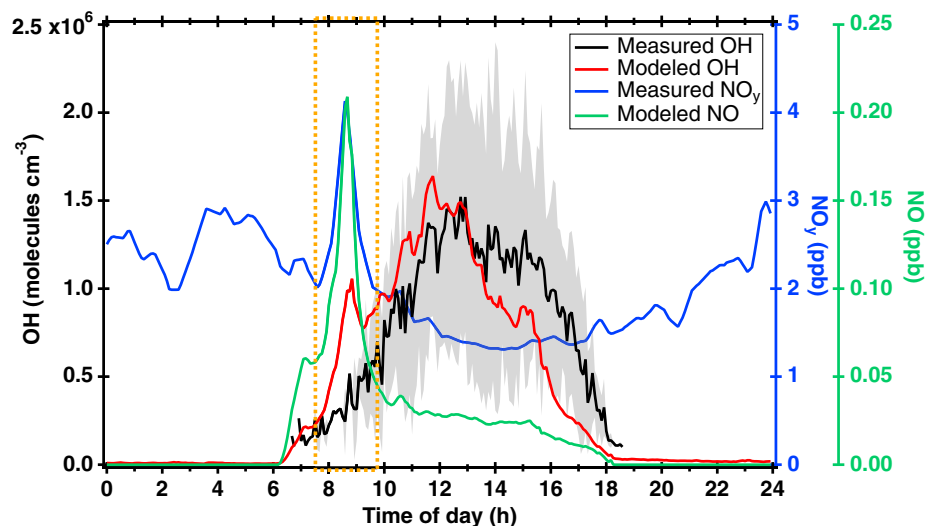


**Figure 6.** Comparison of observed and modeled OH from MCM v3.3.1 box model, shown with measured  $\text{NO}_y$  and modeled NO. The figure shows diurnal variations averaged over the selected days (i.e., 12, 13, 16, 19 February, 9, 15 March), which showed enhanced modeled OH peak in the early morning. The gray shade is the SD of the 6 days of OH measurements.

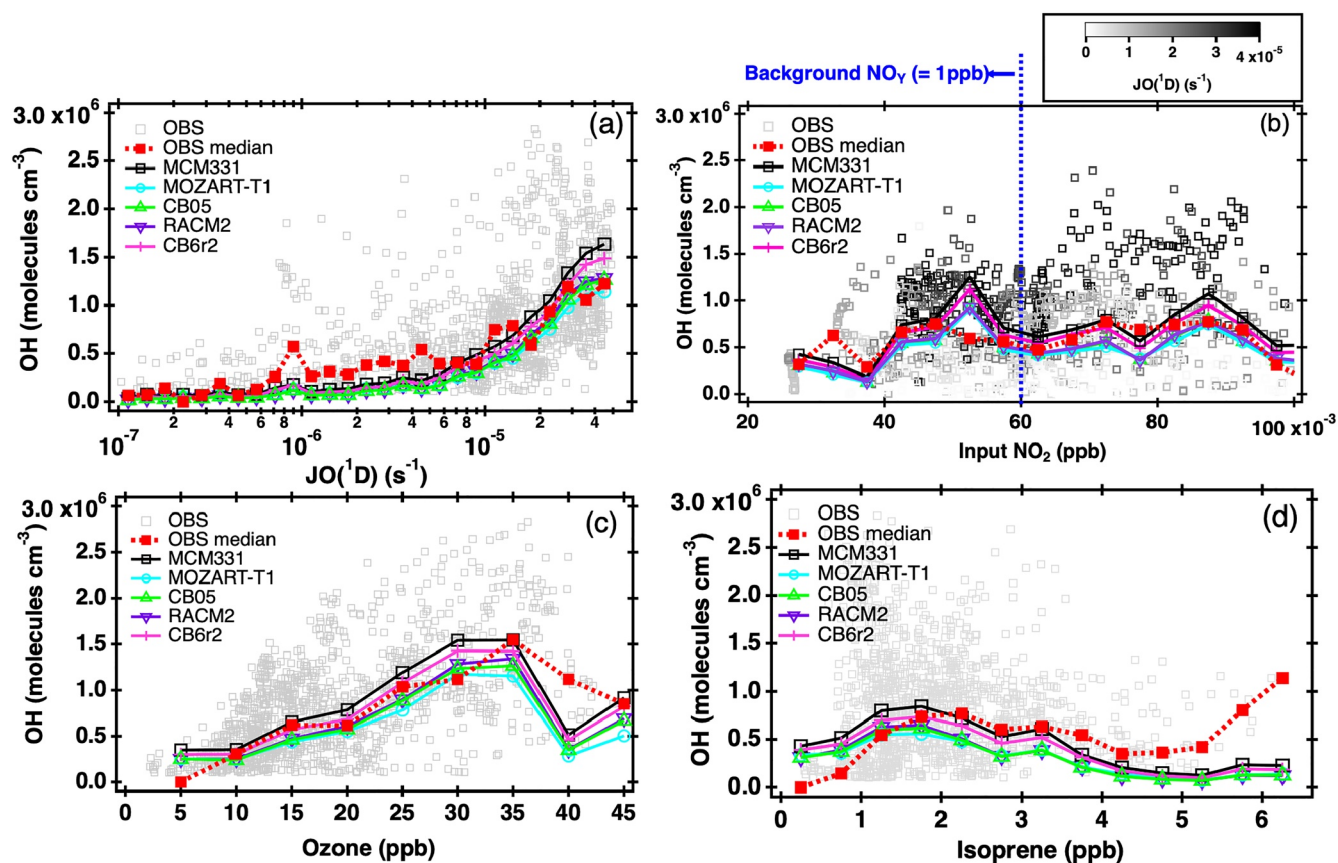


**Figure 7.** Observed and modeled OH with respect to (a)  $O_3$  photolysis rate constant ( $JO^{1D}$ ), (b) model input  $NO_2$ , (c)  $O_3$ , and (d) isoprene. Lines with markers are binned medians of observed and modeled OH. Gray square markers are 5 min averaged OH observation data above the detection limit for (a), (c), and (d). Figure 7b shows results of correlation between OH observations and input  $NO_2$  below 100 ppt. Gray square markers in (b) includes data below LOD and color coded with calculated  $JO^{1D}$  (Results above 100 ppt of input  $NO_2$  are shown in Figure S6).

coefficient for ISOPPOO +  $HO_2$  than MCM v3.3.1 (Wolfe, Kaiser, et al., 2016) but this did not compensate the difference. Other mechanisms simulated  $HO_2$  levels similar to MCM v3.3.1 and show that the radical chemistry is comparable between these mechanisms embedded with the observations during the GoAmazon2014/5. Modeled NO from RACM2 was slightly higher (<7%, Figure S7a) than MCM v3.3.1, which could be due to slower loss rates from  $NO + HO_2$ . This resulted in ~25% less OH production rate from  $NO + HO_2$  in RACM2 compared to other mechanisms (Figure 8d). OH production rate from  $O_3$  photolysis was 20% higher in RACM2 and 11% higher in CB05 compared to MCM v3.3.1 and CB6r2. Since  $O_3$  concentrations and photolysis rate constants ( $J_{O1D}$ ) were constrained identical in all the chemical mechanisms, production rate of  $O^1D$  was the same in all four mechanisms (Figure S7b). However,  $O^1D$  loss rates from quenching reaction to  $O^3P$  were not identical due to differences in reaction coefficients, which were up to 11% (Figure S7b). Moreover, the reaction constant of  $O^1D$  reaction with  $H_2O$  to produce two OH was 3% higher in RACM2 than in MCM v3.3.1. Overall, these discrepancies in the reaction constants contributed up to 20% higher OH production rate from RACM2 from  $O^1D + H_2O$  compared to MCM v3.3.1 and CB6r2. Nonetheless, OH production rate in the “others” category in MCM v3.3.1 was up to a factor of five higher than other mechanisms (Figure 8d), which compensated for the slower rates in the inorganic reactions and resulted in the highest total OH production rate. This is most possibly due to the additional isoprene reactions in the MCM v3.3.1 (Jenkin et al., 2015), which has been updated with the recent theoretical and laboratory studies (Berndt et al., 2019; Crouse et al., 2011; Peeters et al., 2014; Teng et al., 2017). This isoprene scheme has not been updated in the condensed chemical mechanisms used in our study. For comparison, OH simulations were carried out with the MCM v3.2 with model constraints identical to the MCM v3.3.1 simulations. The MCM v3.2 does not include the recent isoprene isomerization reactions and showed ~20% less midday (11:00–13:00) OH than MCM v3.3.1 (Figure S8). In conclusion, the five different chemical mechanisms mostly accounted for observed OH levels during the first IOP of the GoAmazon2014/5 campaign. However, there

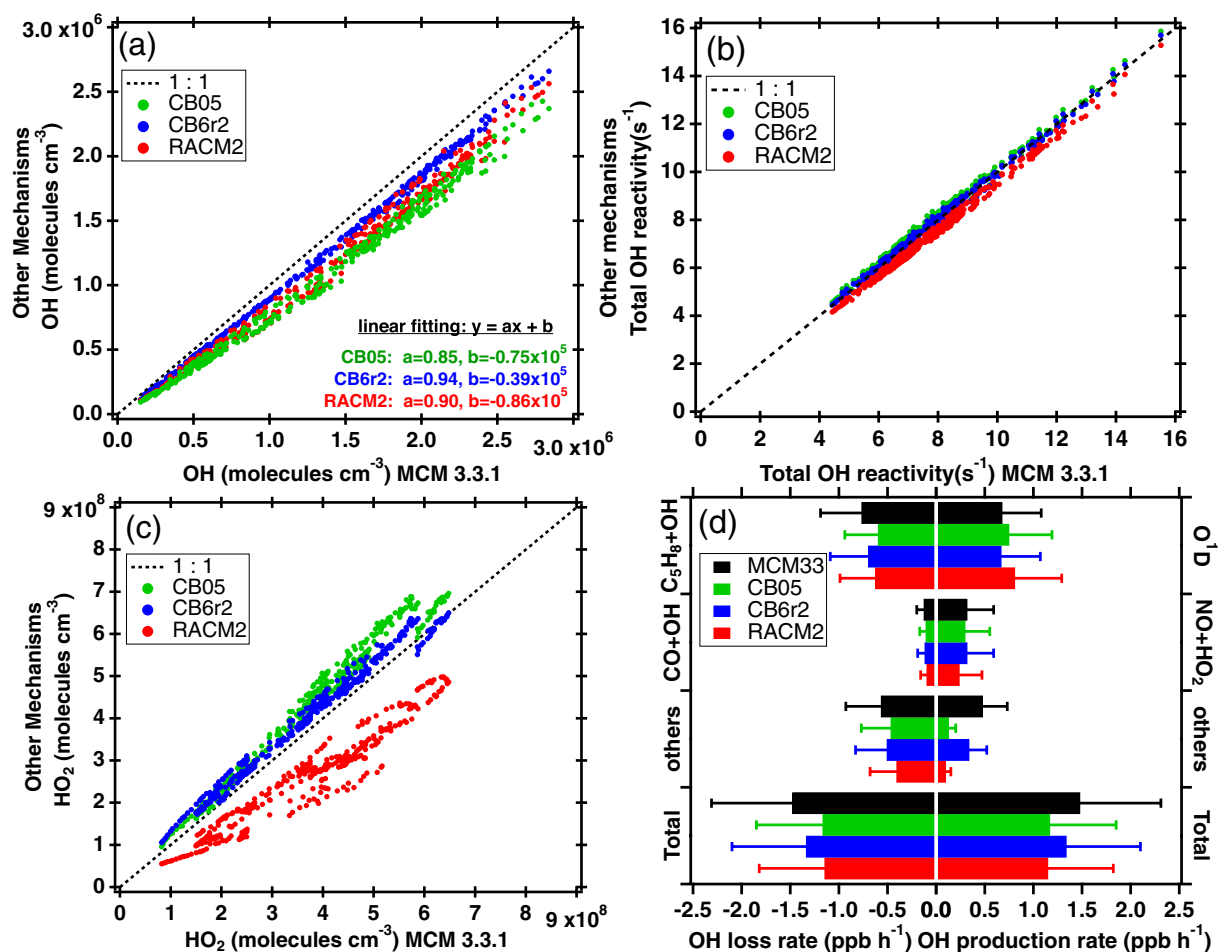


**Figure 8.** Correlation plots between MCM v3.3.1 and other mechanisms of midday (11:00–13:00) (a) modeled OH, (b) modeled total OH reactivity, and (c) modeled HO<sub>2</sub>. (d) OH production and loss rates from model runs embedded with different mechanisms. The rates are averaged over midday and standard deviation of the midday averaged rates of the 14 selected days are shown.

were systematic differences between the chemical mechanisms in treating fundamental radical photochemistry in addition to differences in the isoprene isomerization reactions confirmed in recent laboratory and chamber studies, which is worth noting on evaluating regional and global photochemistry.

#### 4. Conclusions

In this study, we reported OH observations measured with a CIMS in a rainforest during the GoAmazon2014/5. The OH levels observed were similar to previous field observations that used the LIF technique with the chemical removal method. Agreement within the instrumental uncertainty was found between measured OH and box model simulations embedded with near-explicit and four other condensed mechanisms used in chemical transport models. This contrasts with previous studies that reported higher than expected OH levels in forested regions, but consistent with recent results by Mao et al. (2012) and Feiner et al. (2016), where they measured OH with the modified LIF technique during BEARPEX09 and SOAS campaigns. However, the OH reactivity during GoAmazon2014/5 were substantially lower than some of the previous studies that reported significant discrepancy between modeled and measured OH. It is possible that additional unknown OH from understudied isoprene mechanisms could lead to a higher discrepancy in higher OH reactivity conditions. Moreover, BVOCs that are not measured or not identified could contribute to higher OH reactivity. Future studies at the site that encompasses a wider range of BVOC emissions and measurements of total OH reactivity would help further investigation.

Additionally, uncertainties in model simulations remain, for example, in model constraints and rate coefficients. NO<sub>x</sub> observation data set during the campaign was not available due to logistical difficulties and detection limit of the instrument. Therefore, it was estimated from measured NO<sub>y</sub> in the model assuming background conditions. Modeled OH was sensitive to constrained NO<sub>x</sub> levels, which highlights the importance of development of NO<sub>x</sub> measurement techniques that can be implemented in low NO<sub>x</sub> environments to more accurately simulate OH. The model simulations presented in our study showed agreement within instrumental uncertainty of measured OH in the environmental conditions observed during the campaign, which encompasses both background (35%) and polluted NO<sub>y</sub> conditions. However, we acknowledge that the lack of NO<sub>x</sub> measurements is a critical limitation of our analysis. Different chemical mechanisms showed distinct OH production rates from OH recycling (HO<sub>2</sub> + NO) and primary production (H<sub>2</sub>O + O (<sup>1</sup>D)), which could also be a source of uncertainty. MCM v3.3.1 showed higher levels of modeled OH compared to condensed mechanisms that do not include recent laboratory findings of isoprene isomerization reactions. Overall, while uncertainty remains, the observation and model results show good agreement within the instrumental uncertainty of 40% in the photochemical environment during the GoAmazon2014/5 study. Future field studies in a wider range of OH reactivity conditions, for example, during different seasons, with reliable NO<sub>x</sub> measurements will further enhance our understandings and better clarify the uncertainties presented in our study.

## Data Availability Statement

GoAmazon2014/5 data used in this study are available at [www.arm.gov/campaigns/amf2014goamazon](http://www.arm.gov/campaigns/amf2014goamazon).

## Acknowledgments

Institutional support was provided by the Central Office of the Large Scale Biosphere Atmosphere Experiment in Amazonia (LBA), the National Institute of Amazonian Research (INPA), and Amazonas State University (UEA). The authors acknowledge the Atmospheric Radiation Measurement (ARM) Climate Research Facility, a user facility of the United States Department of Energy, Office of Science, sponsored by the Office of Biological and Environmental Research, and support from the Atmospheric System Research (ASR) program of that office. Funding was obtained from the United States Department of Energy (DOE, DESC00011122), the Amazonas State Research Foundation (FAPEAM), the Sao Paulo Research Foundation (FAPESP), the Brazilian Scientific Mobility Program (C&F/CAPES), and the United States National Science Foundation (NSF). The research was conducted under Scientific License 001030/2012-4 of the Brazilian National Council for Scientific and Technological Development (CNPq). This material is based upon work supported by the National Center for Atmospheric Research, which is a major facility sponsored by the NSF under Cooperative Agreement No. 1852977. The AP-CIMS deployed for this field campaign was loaned by National Center for Atmospheric Research (NCAR) in Boulder, Colorado, USA. The authors would like to thank Dr. Glenn M. Wolfe at NASA GSFC for the discussions on the manuscript and model simulations and Dr. Camille Mouchel-Vallon and Dr. Duseong Jo at NCAR ACOM for help on the NCAR box model BOXMOX.

## References

- Alaghmand, M., Shepson, P. B., Starn, T. K., Jobson, B. T., Wallace, H. W., Carroll, M. A., et al. (2011). The Morning NO<sub>x</sub> maximum in the forest atmosphere boundary layer. *Atmospheric Chemistry and Physics Discussions*, 11(10), 29251–29282. <https://doi.org/10.5194/acpd-11-29251-2011>
- Archibald, A. T., Cooke, M. C., Utembe, S. R., Shallcross, D. E., Derwent, R. G., & Jenkin, M. E. (2010). Impacts of mechanistic changes on HO<sub>x</sub> formation and recycling in the oxidation of isoprene. *Atmospheric Chemistry and Physics*, 10(17), 8097–8118. <https://doi.org/10.5194/acp-10-8097-2010>
- Asatryan, R., Da Silva, G., & Bozzelli, J. W. (2010). Quantum chemical study of the acrolein (CH<sub>2</sub>CHCHO) + OH + O<sub>2</sub> reactions. *Journal of Physical Chemistry A*, 114(32), 8302–8311. research-article. <https://doi.org/10.1021/jp104828a>
- Bakwin, P. S., Wofsy, S. C., & Fan, S. (1990). Measurements of reactive nitrogen oxides (NO<sub>y</sub>) within and above a tropical forest canopy in the wet season. *Journal of Geophysical Research*, 95(D10), 16765–16772. <https://doi.org/10.1029/jd095id10p16765>
- Bates, K. H., & Jacob, D. J. (2019). A new model mechanism for atmospheric oxidation of isoprene: Global effects on oxidants, nitrogen oxides, organic products, and secondary organic aerosol. *Atmospheric Chemistry and Physics*, 19(14), 9613–9640. <https://doi.org/10.5194/acp-19-9613-2019>
- Berndt, T., Hyttinen, N., Herrmann, H., & Hansel, A. (2019). First oxidation products from the reaction of hydroxyl radicals with isoprene for pristine environmental conditions. *Communications Chemistry*, 2(1), 1–10. <https://doi.org/10.1038/s42004-019-0120-9>
- Butler, T. M., Taraborrelli, D., Brühl, C., Fischer, H., Harder, H., Martinez, M., et al. (2008). Improved simulation of isoprene oxidation chemistry with the ECHAM5/MESy chemistry-climate model: Lessons from the GABRIEL airborne field campaign. *Atmospheric Chemistry and Physics*, 8, 4529–4546. <https://doi.org/10.5194/acp-8-4529-2008>
- Carlaw, N., Creasey, D. J., Harrison, D., Heard, D. E., Hunter, M. C., Jacobs, P. J., et al. (2001). OH and HO<sub>2</sub> radical chemistry in a forested region of north-western Greece. *Atmospheric Environment*, 35(27), 4725–4737. [https://doi.org/10.1016/S1352-2310\(01\)00089-9](https://doi.org/10.1016/S1352-2310(01)00089-9)
- Chen, S., Ren, X., Mao, J., Chen, Z., Brune, W. H., Lefer, B., et al. (2010). A comparison of chemical mechanisms based on TRAMP-2006 field data. *Atmospheric Environment*, 44(33), 4116–4125. <https://doi.org/10.1016/j.atmosenv.2009.05.027>
- Crouse, J. D., Knap, H. C., Ørnø, K., Jørgensen, S., Paulot, F., Kjaergaard, H. G., & Wennberg, P. O. (2012). Atmospheric fate of methacrolein. 1. Peroxy radical isomerization following addition of OH and O<sub>2</sub>. *Journal of Physical Chemistry A*, 116(24), 5756–5762. <https://doi.org/10.1021/jp211560u>
- Crouse, J. D., Paulot, F., Kjaergaard, H. G., & Wennberg, P. O. (2011). Peroxy radical isomerization in the oxidation of isoprene. *Physical Chemistry Chemical Physics*, 13(30), 13607. <https://doi.org/10.1039/c1cp21330j>
- Crouse, J. D., Teng, A., & Wennberg, P. O. (2014). *Experimental constraints on the distribution and fate of peroxy radicals formed in the reactions of isoprene + OH + O<sub>2</sub> presented at the Atmospheric Chemical Mechanisms: Simple Models – Real world Complexities*, University of California.
- Dodge, M. C. (2000). Chemical oxidant mechanisms for air quality modeling: Critical review. *Atmospheric Environment*, 34(12–14), 2103–2130. [https://doi.org/10.1016/S1352-2310\(99\)00461-6](https://doi.org/10.1016/S1352-2310(99)00461-6)
- Feiner, P. A., Brune, W. H., Miller, D. O., Zhang, L., Cohen, R. C., Romer, P. S., et al. (2016). Testing atmospheric oxidation in an Alabama forest. *Journal of the Atmospheric Sciences*, 73(12), 4699–4710. <https://doi.org/10.1175/JAS-D-16-0044.1>
- Fuchs, H., Hofzumahaus, A., Rohrer, F., Bohn, B., Brauers, T., Dorn, H.-P., et al. (2013). Experimental evidence for efficient hydroxyl radical regeneration in isoprene oxidation. *Nature Geoscience*, 6(12), 1023–1026. <https://doi.org/10.1038/ngeo1964>
- Fuchs, H., Tan, Z., Hofzumahaus, A., Broch, S., Dorn, H. P., Holland, F., et al. (2016). Investigation of potential interferences in the detection of atmospheric RO<sub>x</sub> radicals by laser-induced fluorescence under dark conditions. *Atmospheric Measurement Techniques*, 9(4), 1431–1447. <https://doi.org/10.5194/amt-9-1431-2016>
- Goliff, W. S., Stockwell, W. R., & Lawson, C. V. (2013). The regional atmospheric chemistry mechanism, version 2. *Atmospheric Environment*, 68, 174–185. <https://doi.org/10.1016/j.atmosenv.2012.11.038>

- Griffith, S. M., Hansen, R. F., Dusanter, S., Stevens, P. S., Alaghmand, M., Bertman, S. B., et al. (2013). OH and HO<sub>2</sub> radical chemistry during PROPHET 2008 and CABINEX 2009 - Part 1: Measurements and model comparison. *Atmospheric Chemistry and Physics*, *13*(11), 5403–5423. <https://doi.org/10.5194/acp-13-5403-2013>
- Gross, A., & Stockwell, W. R. (2003). Comparison of the EMEP, RADM2 and RACM mechanisms. *Journal of Atmospheric Chemistry*, *44*(2), 151–170. <https://doi.org/10.1023/A:1022483412112>
- Hens, K., Novelli, A., Martinez, M., Auld, J., Axinte, R., Bohn, B., et al. (2014). Observation and modelling of HO<sub>x</sub> radicals in a boreal forest. *Atmospheric Chemistry and Physics*, *14*(16), 8723–8747. <https://doi.org/10.5194/acp-14-8723-2014>
- Hofzumahaus, A., Rohrer, F., Lu, K., Bohn, B., Brauers, T., Chang, C., et al. (2009). Amplified trace gas removal in the troposphere. *Science*, *324*, 1702–1704. <https://doi.org/10.1126/science.1164566>
- Holland, F., Hofzumahaus, A., Schäfer, J., Kraus, A., & Pätz, H. W. (2003). Measurements of OH and HO<sub>2</sub> radical concentrations and photolysis frequencies during BERLIOZ. *Journal of Geophysical Research: Atmospheres*, *108*(4). <https://doi.org/10.1029/2001jd001393>
- Huey, L. G. (2007). Measurement of trace atmospheric species by chemical ionization mass spectrometry: Speciation of reactive nitrogen and future directions. *Mass Spectrometry Reviews*, *26*, 166, 184. <https://doi.org/10.1002/mas.20118>
- Jacob, J., & Wofsy, S. C. (1988). Photochemistry of biogenic emissions over the Amazon forest. *Journal of Geophysical Research*, *93*(D2), 1477–1486. <https://doi.org/10.1029/jd093id02p01477>
- Jenkin, M. E., Hurley, M. D., & Wallington, T. J. (2007). Investigation of the radical product channel of the CH<sub>3</sub>C(O)O<sub>2</sub> + HO<sub>2</sub> reaction in the gas phase. *Physical Chemistry Chemical Physics*, *9*(24), 3149–3162. <https://doi.org/10.1039/b702757e>
- Jenkin, M. E., Hurley, M. D., & Wallington, T. J. (2010). Investigation of the radical product channel of the CH<sub>3</sub>OCH<sub>2</sub>CO<sub>2</sub> + HO<sub>2</sub> reaction in the gas phase. *Journal of Physical Chemistry A*, *114*(1), 408–416. <https://doi.org/10.1021/jp908158w>
- Jenkin, M. E., Young, J. C., & Rickard, A. R. (2015). The MCM v3.3.1 degradation scheme for isoprene. *Atmospheric Chemistry and Physics*, *15*(20), 11433–11459. <https://doi.org/10.5194/acp-15-11433-2015>
- Jeong, D., Seco, R., Gu, D., Lee, Y., Nault, B. A., Knote, C. J., et al. (2019). Integration of airborne and ground observations of Nitryl Chloride in the Seoul Metropolitan area and the Implications on regional oxidation capacity during KORUS-AQ 2016. *Atmospheric Chemistry and Physics*, *19*, 12779–12795. <https://doi.org/10.5194/acp-19-12779-2019>
- Jimenez, P., Baldasano, J. M., & Dabdub, D. (2003). Comparison of photochemical mechanisms for air quality modeling. *Atmospheric Environment*, *37*(30), 4179–4194. [https://doi.org/10.1016/S1352-2310\(03\)00567-3](https://doi.org/10.1016/S1352-2310(03)00567-3)
- Kaiser, J., Skog, K. M., Baumann, K., Bertman, S. B., Brown, S. B., Brune, W. H., et al. (2016). Speciation of OH reactivity above the canopy of an isoprene-dominated forest. *Atmospheric Chemistry and Physics*, *16*(14), 9349–9359. <https://doi.org/10.5194/acp-16-9349-2016>
- Kim, S., Guenther, A., Lefer, B., Flynn, J., Griffin, R., Rutter, A. P., et al. (2015). Potential role of stabilized criegee radicals in sulfuric acid production in a high biogenic VOC environment. *Environmental Science and Technology*, *49*(6), 3383–3391. <https://doi.org/10.1021/es505793t>
- Kim, S., Kim, S. Y., Lee, M., Shim, H., Wolfe, G. M., Guenther, A. B., et al. (2015). Impact of isoprene and HONO chemistry on ozone and OVOC formation in a semirural South Korean forest. *Atmospheric Chemistry and Physics*, *15*(8), 4357–4371. <https://doi.org/10.5194/acp-15-4357-2015>
- Kim, S., Sanchez, D., Wang, M., Seco, R., Jeong, D., Hughes, S., et al. (2016). OH reactivity in urban and suburban regions in Seoul, South Korea—an East Asian megacity in a rapid transition. *Faraday Discussions*, *189*, 231–251. <https://doi.org/10.1039/c5fd00230c>
- Knote, C., Hodzic, A., Jimenez, J. L., Volkamer, R., Orlando, J. J., Baidar, S., et al. (2014). Simulation of semi-explicit mechanisms of SOA formation from glyoxal in aerosol in a 3-D model. *Atmospheric Chemistry and Physics*, *14*(12), 6213–6239. <https://doi.org/10.5194/acp-14-6213-2014>
- Knote, C., Tuccella, P., Curci, G., Emmons, L., Orlando, J. J., Madronich, S., et al. (2015). Influence of the choice of gas-phase mechanism on predictions of key gaseous pollutants during the AQMEII phase-2 intercomparison. *Atmospheric Environment*, *115*, 553–568. <https://doi.org/10.1016/j.atmosenv.2014.11.066>
- Kubistin, D., Harder, H., Martinez, M., Rudolf, M., Sander, R., Bozem, H., et al. (2010). Hydroxyl radicals in the tropical troposphere over the Suriname rainforest: Comparison of measurements with the box model MECCA. *Atmospheric Chemistry and Physics*, *10*(19), 9705–9728. <https://doi.org/10.5194/acp-10-9705-2010>
- Kuhn, M., Builtjes, P. J. H., Poppe, D., Simpson, D., Stockwell, W. R., Andersson-Sköld, Y., et al. (1998). Intercomparison of the gas-phase chemistry in several chemistry and transport models. *Atmospheric Environment*, *32*(4), 693–709. [https://doi.org/10.1016/S1352-2310\(97\)00329-4](https://doi.org/10.1016/S1352-2310(97)00329-4)
- Kürten, A., Rondo, L., Ehrhart, S., & Curtius, J. (2011). Performance of a corona ion source for measurement of sulfuric acid by chemical ionization mass spectrometry. *Atmospheric Measurement Techniques*, *4*(3), 437–443. <https://doi.org/10.5194/amt-4-437-2011>
- Lelieveld, J., Butler, T. M., Crowley, J. N., Dillon, T. J., Fischer, H., Ganzeveld, L., et al. (2008). Atmospheric oxidation capacity sustained by a tropical forest. *Nature*, *452*(7188), 737–740. <https://doi.org/10.1038/nature06870>
- Levy, H. (1971). Normal atmosphere: Large radical and Formaldehyde concentrations predicted. *Science*, *173*(3992), 141–143. <https://doi.org/10.1126/science.173.3992.141>
- Liao, J., Huey, L. G., Liu, Z., Tanner, D. J., Cantrell, C. A., Orlando, J. J., et al. (2014). High levels of molecular chlorine in the Arctic atmosphere. *Nature Geoscience*, *7*(2), 91–94. <https://doi.org/10.1038/ngeo2046>
- Liao, J., Huey, L. G., Tanner, D. J., Brough, N., Brooks, S., Dibb, J. E., et al. (2011). Observations of hydroxyl and peroxy radicals and the impact of BrO at Summit, Greenland in 2007 and 2008. *Atmospheric Chemistry and Physics*, *11*(16), 8577–8591. <https://doi.org/10.5194/acp-11-8577-2011>
- Liao, J., Huey, L. G., Tanner, D. J., Flocke, F. M., Orlando, J. J., Neuman, J. A., et al. (2012). Observations of inorganic bromine (HOBr, BrO, and Br<sub>2</sub>) speciation at Barrow, Alaska, in spring 2009. *Journal of Geophysical Research: Atmospheres*, *117*(6), 1–11. <https://doi.org/10.1029/2011JD016641>
- Liu, Y., Brito, J., Dorris, M. R., Rivera-Rios, J. C., Seco, R., Bates, K. H., et al. (2016). Isoprene photochemistry over the Amazon rainforest. *Proceedings of the National Academy of Sciences*, *113*(22), 6125–6130. <https://doi.org/10.1073/pnas.1524136113>
- Liu, Y., Seco, R., Kim, S., Guenther, A. B., Goldstein, A. H., Keutsch, F. N., et al. (2018). Isoprene photo-oxidation products quantify the effect of pollution on hydroxyl radicals over Amazonia. *Science Advances*, *4*(4), 1–9. <https://doi.org/10.1126/sciadv.aar2547>
- Logan, J. A., Prather, M. J., Wofsy, S. C., & Mc Elroy, M. B. (1981). Tropospheric chemistry: A global perspective. *Journal of Geophysical Research*, *86*(C8), 7210–7254. <https://doi.org/10.1029/JC086iC08p07210>
- Madronich, S., & Flocke, S. (1998). Handbook of environmental chemistry. In *Handbook of environmental chemistry* (P. Boule, pp. 1–26). Springer\_Verlag.
- Mao, J., Ren, X., Zhang, L., Van Duin, D. M., Cohen, R. C., Park, J. H., et al. (2012). Insights into hydroxyl measurements and atmospheric oxidation in a California forest. *Atmospheric Chemistry and Physics*, *12*(17), 8009–8020. <https://doi.org/10.5194/acp-12-8009-2012>



- Martin, S. T., Artaxo, P., Machado, L., Manzi, A. O., Souza, R. A. F., Schumacher, C., et al. (2017). *The Green Ocean Amazon experiment (GoAmazon2014/5) Observes pollution affecting gases, aerosols, Clouds, and Rainfall over the rain forest*. Bulletin of the American Meteorological Society. <https://doi.org/10.1175/BAMS-D-15-00221.1>
- Martin, S. T., Artaxo, P., MacHado, L. A. T., Manzi, A. O., Souza, R. A. F., Schumacher, C., et al. (2016). Introduction: Observations and modeling of the Green Ocean Amazon (GoAmazon2014/5). *Atmospheric Chemistry and Physics*, 16(8), 4785–4797. <https://doi.org/10.5194/acp-16-4785-2016>
- Mauldin, R. L., Frost, G. J., Chen, G., Tanner, D. J., Prevot, A. S. H., Davis, D. D., & Eisele, F. L. (1998). OH measurements during the first aerosol characterization experiment (ACE 1): Observations and model comparisons. *Journal of Geophysical Research: Atmospheres*, 103(D13), 16713–16729. <https://doi.org/10.1029/98JD00882>
- Mauldin, R. L., Kosciuch, E., Henry, B., Eisele, F. L., Shetter, R., Lefer, B., et al. (2010). Measurements of OH, HO<sub>2</sub>+RO<sub>2</sub>, H<sub>2</sub>SO<sub>4</sub>, and MSA at the South Pole during ISCAT 2000. *Advances in Horticultural Science*, 24(1), 43–52. <https://doi.org/10.1016/j.atmosenv.2004.06.031>
- Nolscher, A. C., Yanez-Serrano, A. M., Wolff, S., Carioca de Araujo, A., Lavric, J. V., Kesselmeier, J., Williams, J. (2016). Unexpected seasonality in quantity and composition of Amazon rainforest air reactivity. *Nature Communications*, 7, 1–12(1038). <https://doi.org/10.1038/ncomms10383>
- Novelli, A., Hens, K., Ernest, C. T., Martinez, M., Nölscher, A. C., Sinha, V., et al. (2017). Estimating the atmospheric concentration of Criegee intermediates and their possible interference in a FAGE-LIF instrument. *Atmospheric Chemistry and Physics*, 17(12), 7807–7826. <https://doi.org/10.5194/acp-17-7807-2017>
- Novelli, A., Hens, K., Tatum Ernest, C., Kubistin, D., Regelin, E., Elste, T., et al. (2014). Characterisation of an inlet pre-injector laser-induced fluorescence instrument for the measurement of atmospheric hydroxyl radicals. *Atmospheric Measurement Techniques*, 7(10), 3413–3430. <https://doi.org/10.5194/amt-7-3413-2014>
- Novelli, A., Kaminski, M., Rolletter, M., Acir, I. H., Bohn, B., Dorn, H. P., et al. (2018). Evaluation of OH and HO<sub>2</sub> concentrations and their budgets during photooxidation of 2-methyl-3-butene-2-ol (MBO) in the atmospheric simulation chamber SAPHIR. *Atmospheric Chemistry and Physics*, 18(15), 11409–11422. <https://doi.org/10.5194/acp-18-11409-2018>
- Novelli, A., Vereecken, L., Bohn, B., Dorn, H. P., Gkatzelis, G. I., Hofzumahaus, A., et al. (2020). Importance of isomerization reactions for OH radical regeneration from the photo-oxidation of isoprene investigated in the atmospheric simulation chamber SAPHIR. *Atmospheric Chemistry and Physics*, 20(6), 3333–3355. <https://doi.org/10.5194/acp-20-3333-2020>
- Peeters, J. (2015). Interactive comment on “The MCM v3.3. Degradation scheme for isoprene” by M. E. Jenkin et al., *Atmospheric Chemistry and Physics Discussions*, 15, C2486.
- Peeters, J., & Müller, J. F. (2010). HOx radical regeneration in isoprene oxidation via peroxy radical isomerisations. II: Experimental evidence and global impact. *Physical Chemistry Chemical Physics*, 12(42), 14227. <https://doi.org/10.1039/c0cp00811g>
- Peeters, J., Müller, J. F., Stavrou, T., & Nguyen, V. S. (2014). Hydroxyl radical recycling in isoprene oxidation driven by hydrogen bonding and hydrogen tunneling: The upgraded LIM1 mechanism. *Journal of Physical Chemistry A*, 118(38), 8625–8643. <https://doi.org/10.1021/jp5033146>
- Peeters, J., Nguyen, T. L., & Vereecken, L. (2009). HOx radical regeneration in the oxidation of isoprene. *Physical Chemistry Chemical Physics*, 11(28), 5935. <https://doi.org/10.1039/b908511d>
- Pugh, T. A. M., MacKenzie, A. R., Hewitt, C. N., Langford, B., Edwards, P. M., Furneaux, K. L., et al. (2010). Simulating atmospheric composition over a South-East Asian tropical rainforest: Performance of a chemistry box model. *Atmospheric Chemistry and Physics*, 10, 279–298. <https://doi.org/10.5194/acp-10-279-2010>
- Raso, A. R. W., Custard, K. D., May, N. W., Tanner, D., Newburn, M. K., Walker, L., et al. (2017). Active molecular iodine photochemistry in the Arctic. *Proceedings of the National Academy of Sciences*, 114(38), 10053–10058. <https://doi.org/10.1073/pnas.1702803114>
- Ren, X., Olson, J. R., Crawford, J. H., Brune, W. H., Mao, J., Long, R. B., et al. (2008). HOx chemistry during INTEX-A 2004: Observation, model calculation, and comparison with previous studies. *Journal of Geophysical Research: Atmospheres*, 113(5), 1–13. <https://doi.org/10.1029/2007JD009166>
- Rickly, P., & Stevens, P. S. (2018). Measurements of a potential interference with laser-induced fluorescence measurements of ambient OH from the ozonolysis of biogenic alkenes. *Atmospheric Measurement Techniques*, 11(1), 1–16. <https://doi.org/10.5194/amt-11-1-2018>
- Rohrer, F., Lu, K., Hofzumahaus, A., Bohn, B., Brauers, T., Chang, C. C., et al. (2014). Maximum efficiency in the hydroxyl-radical-based self-cleansing of the troposphere. *Nature Geoscience*, 7(8), 559–563. <https://doi.org/10.1038/ngeo2199>
- Ruiz, L. H., & Yarwood, G. (2013). Prepared for the Texas AQRP (Project 12-012) University of Texas at Austin, and ENVIRON International Corporation; 2013. Interactions between organic aerosol and NOy: Influence on oxidant production.
- Sanchez, D., Jeong, D., Seco, R., Wrangham, I., Park, J. H., Brune, W. H., et al. (2018). Intercomparison of OH and OH reactivity measurements in a high isoprene and low NO environment during the Southern Oxidant and Aerosol Study (SOAS). *Atmospheric Environment*, 174, 227–236. <https://doi.org/10.1016/j.atmosenv.2017.10.056>
- Saunders, S. M., Jenkin, M. E., Derwent, R. G., & Pilling, M. J. (1997). World Wide Web site of a master chemical mechanism (MCM) for use in tropospheric chemistry models. *Atmospheric Environment*, 31(8), 1249. [https://doi.org/10.1016/S1352-2310\(97\)85197-7](https://doi.org/10.1016/S1352-2310(97)85197-7)
- Saunders, S. M., Jenkin, M. E., Derwent, R. G., & Pilling, M. J. (2003). Protocol for the development of the master chemical mechanism, MCM v3 (Part A): Tropospheric degradation of non-aromatic volatile organic compounds. *Atmospheric Chemistry and Physics*, 3(1), 161–180. <https://doi.org/10.5194/acp-3-161-2003>
- Sjostedt, S. J., Huey, L. G., Tanner, D. J., Peischl, J., Chen, G., Dibb, J. E., et al. (2007). Observations of hydroxyl and the sum of peroxy radicals at Summit, Greenland during summer 2003. *Atmospheric Environment*, 41(24), 5122–5137. <https://doi.org/10.1016/j.atmosenv.2006.06.065>
- Stone, D., Evans, M. J., Commane, R., Ingham, T., Floquet, C. F. A., McQuaid, J. B., et al. (2010). HOx observations over west Africa during AMMA: Impact of isoprene and NOx. *Atmospheric Chemistry and Physics*, 10(19), 9415–9429. <https://doi.org/10.5194/acp-10-9415-2010>
- Tan, D., Faloon, I., Simpas, J. B., Brune, W., Shepson, P. B., Couch, T. L., et al. (2001). HOx budgets in a deciduous forest: Results from the PROPHET summer 1998 campaign. *Journal of Geophysical Research: Atmospheres*, 106(D20), 24407–24427. <https://doi.org/10.1029/2001JD900016>
- Tan, Z., Fuchs, H., Lu, K., Hofzumahaus, A., Bohn, B., Broch, S., et al. (2017). Radical chemistry at a rural site (Wangdu) in the North China Plain: Observation and model calculations of OH, HO<sub>2</sub> and RO<sub>2</sub> radicals. *Atmospheric Chemistry and Physics*, 17(1), 663–690. <https://doi.org/10.5194/acp-17-663-2017>
- Tanner, D. J., Jefferson, A., & Eisele, F. L. (1997). Selected ion chemical ionization mass spectrometric measurement of OH. *Journal of Geophysical Research: Atmospheres*, 102(D5), 6415–6425. Doi. <https://doi.org/10.1029/96jd03919>
- Taraborrelli, D., Lawrence, M. G., Butler, T. M., Sander, R., & Lelieveld, J. (2009). Mainz Isoprene Mechanism 2 (MIM2): An isoprene oxidation mechanism for regional and global atmospheric modelling. *Atmospheric Chemistry and Physics*, 9(8), 2751–2777. <https://doi.org/10.5194/acp-9-2751-2009>

- Teng, A. P., Crouse, J. D., & Wennberg, P. O. (2017). Isoprene peroxy radical Dynamics. *Journal of the American Chemical Society*, *139*(15), 5367–5377. <https://doi.org/10.1021/jacs.6b12838>
- Thornton, J. A., Wooldridge, P. J., Cohen, R. C., Martinez, M., Harder, H., Brune, W. H., et al. (2002). Ozone production rates as a function of NO<sub>x</sub> abundances and HO<sub>x</sub> production rates in the Nashville urban plume. *Journal of Geophysical Research*, *107*(D12), 4146. <https://doi.org/10.1029/2001JD000932>
- Wennberg, P. O., Bates, K. H., Crouse, J. D., Dodson, L. G., McVay, R. C., Mertens, L. A., et al. (2018). Gas-phase reactions of isoprene and its major oxidation products. *Chemical Reviews*, *118*(7), 3337–3390. <https://doi.org/10.1021/acs.chemrev.7b00439>
- Whalley, L. K., Edwards, P. M., Furneaux, K. L., Goddard, A., Ingham, T., Evans, M. J., et al. (2011). Quantifying the magnitude of a missing hydroxyl radical source in a tropical rainforest. *Atmospheric Chemistry and Physics*, *11*(14), 7223–7233. <https://doi.org/10.5194/acp-11-7223-2011>
- Wolfe, G. M., Cantrell, C., Kim, S., Mauldin, R. L., Karl, T., Harley, P., et al. (2014). Missing peroxy radical sources within a summertime ponderosa pine forest. *Atmospheric Chemistry and Physics*, *14*(9), 4715–4732. <https://doi.org/10.5194/acp-14-4715-2014>
- Wolfe, G. M., Crouse, J. D., Parrish, J. D., St Clair, J. M., Beaver, M. R., Paulot, F., et al. (2012). Photolysis, OH reactivity and ozone reactivity of a proxy for isoprene-derived hydroperoxyenals (HPALDs). *Physical Chemistry Chemical Physics*, *14*(20), 7276–7286. <https://doi.org/10.1039/c2cp40388a>
- Wolfe, G. M., Kaiser, J., Hanisco, T. F., Keutsch, F. N., De Gouw, J. A., Gilman, J. B., et al. (2016). Formaldehyde production from isoprene oxidation across NO<sub>x</sub> regimes. *Atmospheric Chemistry and Physics*, *16*(4), 2597–2610. <https://doi.org/10.5194/acp-16-2597-2016>
- Wolfe, G. M., Marvin, M. R., Roberts, S. J., Travis, K. R., & Liao, J. (2016). The framework for 0-D atmospheric modeling (F0AM) v3.1. *Geoscientific Model Development*, *9*(9), 3309–3319. <https://doi.org/10.5194/gmd-9-3309-2016>
- Yarwood, G., Whitten, G., & Rao, S. (2005). *Updates to the Carbon Bond 4 photochemical mechanism prepared for Lake Michigan air directors consortium*.
- Zimmerman, P. R., Greenberg, J. P., & Westberg, C. E. (1988). Measurements of atmospheric hydrocarbons and biogenic emission fluxes in the Amazon Boundary layer. *Journal of Geophysical Research: Atmospheres*, *93*(D2), 1407–1416. <https://doi.org/10.1029/JD093iD02p01407>

## References From the Supporting Information

- Chen, Q., Fan, J., Hagos, S., Gustafson, W. I., & Berg, L. K. (2015). Roles of wind shear at different vertical levels: Cloud system organization and properties. *Journal of Geophysical Research: Atmospheres*, *120*(13), 6551–6574. <https://doi.org/10.1002/2015JD023253>
- Flynn, C. J. (2016). *Shortwave Array Spectroradiometer–Hemispheric (SASHe) instrument Handbook*. <https://doi.org/10.2172/1251414>
- Graus, M., Muller, M., & Hansel, A. (2010). High resolution PTR-TOF: Quantification and Formula Confirmation of VOC in real time. *Journal of the American Society for Mass Spectrometry*, *21*(6), 1037–1044. <https://doi.org/10.1016/j.jasms.2010.02.006>
- Greenberg, J. P., & Zimmerman, P. R. (1984). Nonmethane hydrocarbons in remote tropical, continental, and marine atmospheres. *Journal of Geophysical Research*, *89*(D3), 4767–4778. <https://doi.org/10.1029/JD089iD03p04767>
- Jordan, A., Haidacher, S., Hanel, G., Hartungen, E., Märk, L., Seehauser, H., et al. (2009). A high resolution and high sensitivity proton-transfer-reaction time-of-flight mass spectrometer (PTR-TOF-MS). *International Journal of Mass Spectrometry*, *286*(2–3), 122–128. <https://doi.org/10.1016/j.ijms.2009.07.005>